Izvestiya, Physics of the Solid Earth, Vol. 39, No. 9, 2003, pp. 701–727. Translated from Fizika Zemli, No. 9, 2003, pp. 3–30.

Magnetovariational Sounding: New Possibilities

M. N. Berdichevsky, V. I. Dmitriev, N. S. Golubtsova, N. A. Mershchikova, and P. Yu. Pushkarev

Moscow State University, Vorob'evy gory, Moscow, 119899 Russia

Received May 6, 2003

Abstract—Geoelectric research provides unique information on the stratification of the Earth and its deep structures. A basic geoelectric method is believed to be magnetotelluric sounding (MTS), underlain by the inversion of frequency responses of the impedance tensor, which are determined from the electric and magnetic fields. The MTS data interpretation is complicated due to near-surface inhomogeneities distorting the electric field. Modern geoelectric methods allow more or less reliable identification of these distortions and their elimination. The MTS method is complemented by magnetovariational profiling (MVP) using the tipper (the Wiese-Parkinson vector), which is determined from the magnetic field alone. The MVP role reduces to the recognition and localization of geoelectric structures disturbing the horizontal homogeneity of the medium studied. However, the theorem of uniqueness proved in this paper for the 2-D magnetovariational inversion problem indicates that the tipper not only reflects the geoelectric asymmetry of the medium but also provides constraints on its stratification, i.e., enables the construction of layered inhomogeneous sections. Thus, local magnetovariational sounding (MVS) based on the straightforward inversion of frequency responses of the tipper can be applied together with the MTS. The main distinctive MVS feature is the fact that distortions of the magnetic field caused by near-surface inhomogeneities attenuate with decreasing frequency and do not spoil the information on deep structures. Evidently, local MVS allows one to avoid the difficulties inherent in the MTS due to the near-surface distortion of apparent resistivity curves, which are constructed from frequency responses of the impedance tensor. We arrive at the conclusion that MVS can substantially improve the reliability of geoelectric reconstructions. In this respect, several problems related to the combination of the MVS and MTS methods arise. In this paper, we analyze an MVS–MTS complex in which the MVS plays the role of a basic method and the MTS is employed for checking and refining MVS data. An algorithm based on the principle of successive inversions is proposed for the integrated interpretation of MVS and MTS characteristics. The paper consists of theoretical and experimental parts. The uniqueness theorem is proven in the theoretical part for the 2-D MVS inversion problem. The experimental part of the paper describes model experiments on the interpretation of MVS and MTS synthetic data and presents a geoelectric model of the Cascadian subduction zone constrained primarily by MVS data.

INTRODUCTION

Modern magnetotellurics consists of two interrelated approaches: (i) the magnetotelluric sounding (MTS) based on the simultaneous measurements of the electric (telluric) and magnetic fields of the Earth and (ii) the magnetovariational sounding (MVS) restricted to the measurements of magnetic field variations alone [Rokityansky, 1982; Berdichevsky and Zhdanov, 1984; Vozoff, 1991; Berdichevsky and Dmitriev, 2002].

Main MTS characteristics are the impedance tensor [**Z**], determined from relations between the horizontal components of the electric and magnetic fields,

$$\mathbf{E}_\tau = [\mathbf{Z}]\mathbf{H}_\tau, \qquad (1)$$

where

$$\mathbf{E}_\tau = \mathbf{E}_\tau(E_x, E_y) \quad [\mathbf{Z}] = \begin{bmatrix} Z_{xx} & Z_{xy} \\ Z_{yx} & Z_{yy} \end{bmatrix},$$

$$\mathbf{H}_\tau = \mathbf{H}_\tau(H_x, H_y),$$

and the apparent resistivities

$$\rho_{xy} = \frac{|Z_{xy}|^2}{\omega\mu_0}, \quad \rho_{yx} = \frac{|Z_{yx}|^2}{\omega\mu_0}, \qquad (2)$$

calculated from the moduli of the off-diagonal components of the impedance tensor.

The main characteristic of the MVS and MVP methods is the tipper [**W**] (the Wiese-Parkinson vector), determined from the relations between the vertical component of the magnetic field and its horizontal components

$$H_z = [\boldsymbol{W}]\mathbf{H}_\tau, \qquad (3)$$

where

$$[\mathbf{W}] = \begin{bmatrix} W_{zx} & W_{zy} \end{bmatrix}.$$

In the traditional scheme of electromagnetic sounding using the magnetotelluric field, the MTS method plays a leading role (stratification of the medium, geoelectric regionalization, mapping of subsurface topog-

raphies, tracing of horizontal variations in the electrical conductivity, and identification of conducting layers in the crust and upper mantle), whereas the MVS method is only employed for the recognition and localization of contrasting structures and for the determination of their strikes [Rokityansky, 1982]. This scheme has been extensively and, in many respects, successfully applied throughout the world, providing unique information on the Earth's interiors (porosity, graphitization and sulfidization, fluid and rheological regimes, dehydration, and melting). Its weak point is the distortion introduced by inhomogeneities of the uppermost layers of the Earth into the electric field and thereby into the apparent resistivity. As the frequency decreases, these effects become galvanic and involve the entire range of low frequencies, distorting the information on the deep electrical conductivity. The galvanic effects give rise to a static (conformal) shift of the low-frequency branches of apparent resistivity curves. Presently, many methods are used for suppressing these effects [Bahr, 1988; Jones, 1988; Groom and Bailey, 1989; Zinger, 1992; Caldwell *et al.*, 2002; Berdichevsky and Dmitriev, 2002]. The most frequent among them are various types of averaging, filtering, reductions to high- and low-frequency references, and model corrections. However, all these techniques involve the risk of overly gross approximations or even subjective (and sometimes erroneous) decisions resulting in structural misidentifications.

This scheme can be substantially improved by using the MVS potentialities. The point is that, with decreasing frequency, the current induced in the Earth involves increasingly deeper layers and the effects of near-surface inhomogeneities on its magnetic field weaken. Using data on the magnetic field alone, one can obtain reasonably reliable information on deep geoelectric structures.

The studies in the field of integrated interpretation of MTS and MVS data are conducted in two directions.

1. Methods of magnetic-to-electric field transformation are being elaborated. In this way, the impedance related to the TE-mode of the magnetotelluric field is determined. The "induction" curves of apparent resistivity constructed with the use of the TE-impedance have nearly undistorted low-frequency branches. The idea of such a transformation was proposed by L.L. Vanyan [Osipova *et al.*, 1982]. The first experiments in this direction were conducted in the early 1980s [Osipova *et al.*, 1982; Bur'yanov *et al.*, 1983]. In recent years, L.L. Vanyan, I.M. Varentsov, N.G. Golubev, and E.Yu. Sokolova have developed algorithms and computer programs for the 2-D TE-impedance determination and carried out the interpretation of the induction curves of apparent resistivity obtained for the western coast of the United States [Vanyan *et al.*, 1997, 1998]. These investigations played an important role in the progress of the EMSLAB experiment, because they substantiated the presence of the asthenosphere in the continental part of the Cascadian subduction zone. The main drawback of such an approach consists in model errors caused by the necessity of a priori specification of a normal (undistorted) impedance. Therefore, the construction of induction curves of apparent resistivity should primarily be regarded as a means for the visualization of MVS data facilitating their analysis (qualitative assessment of the stratification of the medium and geoelectric regionalization).

2. The theory and methods of straightforward MVS data inversion that is based on the minimization of Tikhonov's functional containing the tipper misfit are being developed. This approach goes back to the magnetotelluric experiments that were carried out in 1988–1990 in the Kyrgyz Tien Shan by geophysical teams of the Institute of High Temperatures, Russian Academy of Sciences [Trapeznikov *et al.*, 1997; Berdichevsky and Dmitriev, 2002]. These measurements were made on a profile characterized by strong local and regional distortions of apparent resistivities that complicate the interpretation of resulting data. The situation could be normalized only with MVS soundings. Figure 1 plots the real tippers $\mathrm{Re}\, W_{zy}$ and the geoelectric model fitting these curves. The model crust contains an inhomogeneous conducting layer (a depth interval of 25–55 km) and vertical conducting zones confined to the known faults (the Nikolaev line and the Atbashi-Inylchik fault). The figure also presents the model constructed from seismic tomography data. The geoelectric model is in good agreement with the observations and coincides remarkably well with the seismic model: low resistivities are reliably correlated with lower velocities. This correlation confirms the validity of geoelectric reconstructions based on MVS data. The experimental investigations in the Tien Shan indicate that MVS not only localizes crustal structures but also provides constraints on the stratification of the crust. Developing this inference, we propose a new MVS scheme in which the MVS plays a leading role, whereas MTS data are utilized for a check and a more detailed specification of the MVS results.

This paper is devoted to the problems related to the second direction of research in the MVS theory and methods. We prove the uniqueness of the 2-D MVS data inversion, describe model experiments on joint MVS and MTS data interpretation, and present a new model of the Cascadian subduction zone constructed according to a scheme of successive inversions dominated by MVS data.

UNIQUENESS OF THE MVS INVERSION PROBLEM SOLUTION

The MVS inversion problem is meant here as the reconstruction of the electric conductivity $\sigma(x, y, z)$ from tipper values specified within a wide frequency range on sufficiently long profiles or in a sufficiently large area. The uniqueness of the solution of the inverse

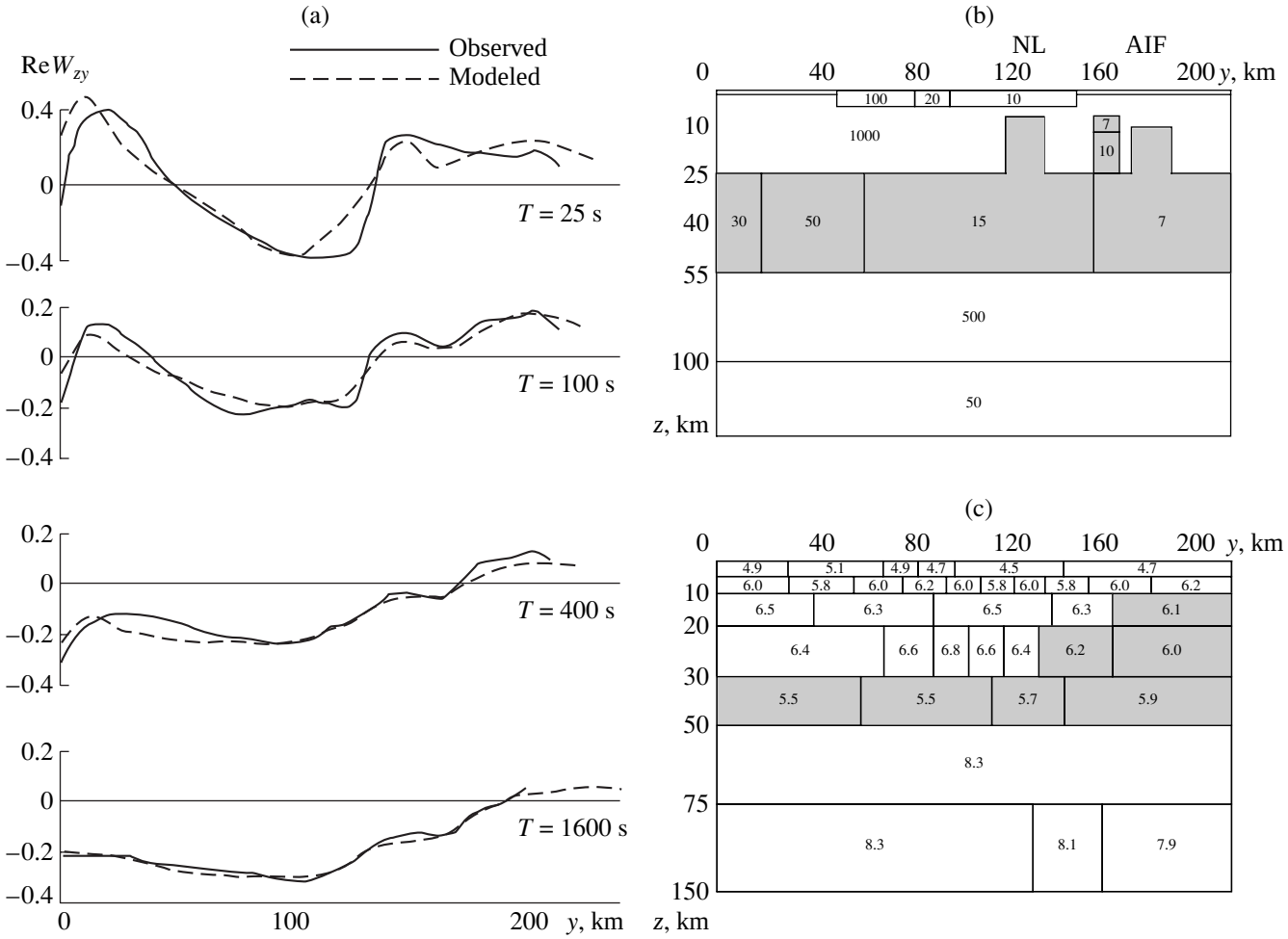

Fig. 1. Magnetovariational sounding in the Kyrgyz Tien Shan Mountains. (a) Plots of the real tipper constructed along a profile crossing the Kyrgyz Tien Shan. (b) The resistivity section constructed from MVS data [Trapeznikov *et al.*, 1997]: NL, Nikolaev line; AIF, Atbashi-Inylchik faults. The resistivity values (in Ω m) are given within blocks; the lower-resistivity crustal zone ($\rho \le 50$ Ωm) is shaded. (c) The velocity section from seismic tomography data [Roecker *et al.*, 1993]. Values of *P* wave velocities (in km/s) are given within blocks; the low-velocity crustal zone ($v_p \le 6.2$ km/s) is shaded.

problem is a key problem of the MVS method, determining its informativeness.

At first glance, MVS anomalies do not seem to provide any information on the normal structure of the medium $\sigma_N(z)$, because we have $W_{zx} = W_{zy} = 0$ in a horizontally homogeneous model. However, in the case of a horizontally inhomogeneous medium, MVS can be considered as frequency sounding that uses the magnetic field of a buried local source. Such a source can be represented by any inhomogeneity $\Delta\sigma(x, y, z)$ in which an excessive electric current spreading in the medium is induced. Evidently, the distribution of this current, as well as its magnetic field, depends not only on the inhomogeneity structure $\Delta\sigma(x, y, z)$ but also on the normal structure of the medium $\sigma_N(z)$. Thus, the solution of the inverse MVS problem $\sigma(x, y, z) = \sigma_N(z) + \Delta\sigma(x, y, z)$ exists and we should examine its uniqueness.

We consider the 2-D model shown in Fig. 2. In this model, a horizontally layered Earth having the normal conductivity

$$\sigma_N(z) = \begin{cases} \sigma(z), & 0 \le z \le H \\ \sigma_H, & H \le z \end{cases} \quad (4)$$

contains a 2-D inhomogeneous region *S* having an excessive conductivity $\Delta\sigma(y, z) = \sigma(y, z) - \sigma_N(z)$. The inhomogeneity is elongated along the *x* axis and its cross section has a maximum size *d*. The functions $\sigma_N(z)$ and $\Delta\sigma(y, z)$ are piecewise-analytical. The region *S* is underlain at a depth *H* by an homogeneous basement of conductivity σ_H = const. The air is an ideal insulator. The magnetic permittivity is equal everywhere to its vacuum value μ_0. The model is excited by a plane electromagnetic wave striking vertically the Earth's

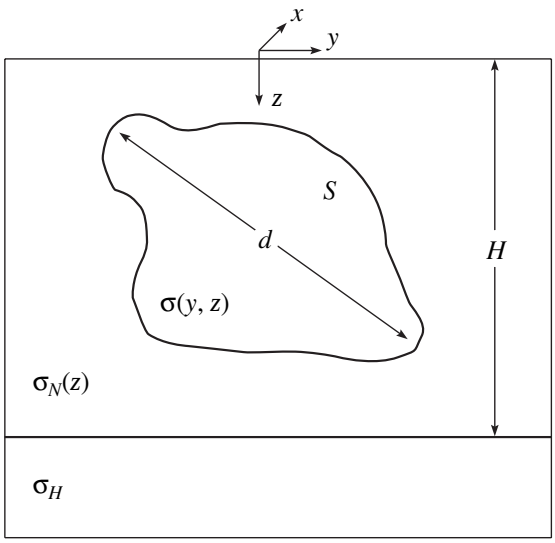

Fig. 2. Model of a horizontally layered medium containing a 2-D inhomogeneous region *S*.

surface. The time dependence of the field is described by the factor $e^{-i\omega t}$.

The uniqueness theorem is formulated for the MVS inverse problem in this model as follows: *the piecewise-analytical distribution of the electrical conductivity*

$$\sigma(M) = \begin{cases} \sigma_N(z) & M \notin S \\ \sigma_N(z) + \Delta\sigma(y, z) & M \in S \end{cases} \tag{5}$$

is uniquely defined by the exact values of the tipper

$$W_{zy}(y) = \frac{H_z(y, z = 0)}{H_y(y, z = 0)}, \quad -\infty < y < \infty, \quad 0 \le \omega < \infty, \tag{6}$$

that are given on the Earth's surface z = 0 at all points of the y axis from –∞ to ∞ for all frequencies ranging from 0 to ∞.

The proof of the uniqueness theorem consists of two stages. First, we consider the asymptotic behavior of the tipper $W_{zy}(y)$ at great distances from the inhomogeneity *S* and show that the frequency response of this asymptotics uniquely determines the normal conductivity distribution $\sigma_N(z)$. Further, we prove that, if $\sigma_N(z)$ is known, the tipper uniquely determines the impedance of the inhomogeneous medium.

An anomalous magnetic field on the Earth's surface can be represented as the field produced in a horizontally homogeneous layered medium by excess currents of the density j_x that are induced in the region *S*:

$$\tilde{H}_y^A(y) = \frac{H_y^A(y, z = 0)}{H_y^N(z = 0)} = \int_S j_x(M_0) h_y(y, M_0) dS,$$
$$\tilde{H}_z(y) = \frac{H_z^A(y, z = 0)}{H_y^N(z = 0)} = \int_S j_x(M_0) h_z(y, M_0) dS, \tag{7}$$

where $h_y(y, M_0)$ and $h_z(y, M_0)$ are the magnetic fields on the surface of the horizontally homogeneous medium produced by a linear current of unit density flowing at a point $M_0(y_0, z_0) \in S$. These functions have the form [Dmitriev, 1969; Berdichevsky and Zhdanov, 1984]

$$h_y(y, M_0) = \frac{i}{\omega\mu_0} \lim_{z \to 0} \int_0^\infty \cos\lambda(y - y_0) e^{\lambda z} \times U(\lambda, z = 0, z_0) \lambda d\lambda, \tag{8}$$

$$h_z(y, M_0) = -\frac{i}{\omega\mu_0} \lim_{z \to 0} \int_0^\infty \sin\lambda(y - y_0) e^{\lambda z} \times U(\lambda, z = 0, z_0) \lambda d\lambda, \tag{9}$$

where the factor $e^{\lambda z}$ relates to the upper half-space $z \le 0$ and the function $U(\lambda, z, z_0)$ is the solution of the boundary value problem

$$\frac{d^2 U(\lambda, z, z_0)}{dz^2} - \eta^2(\lambda, z) U(\lambda, z, z_0) = -\delta(z - z_0),$$
$$z, z_0 \in [0, H],$$
$$\eta(\lambda, z) = \sqrt{\lambda^2 - i\omega\mu_0\sigma_N(z)}, \quad \mathrm{Re}\,\eta > 0,$$
$$\frac{dU(\lambda, z, z_0)}{dz} + \lambda U(\lambda, z, z_0) = 0 \text{ at } z = 0, \tag{10}$$
$$\frac{dU(\lambda, z, z_0)}{dz} - \eta_H(\lambda) U(\lambda, z, z_0) = 0 \text{ at } z = H,$$
$$\eta_H(\lambda) = \sqrt{\lambda^2 - i\omega\mu_0\sigma_H}, \quad \mathrm{Re}\,\eta_H > 0.$$

The anomalous magnetic field components $\tilde{H}_y^A$ and $\tilde{H}_z$ can be found from the tipper values known at all points of the *y* axis [Dmitriev and Mershchikova,

2002]. In order to determine $\tilde{H}_y^A$, we solve the integral equation

$$W_{zy}(y)\tilde{H}_y^A(y) + \frac{1}{\pi}\int_{-\infty}^{\infty}\frac{\tilde{H}_y^A(y_0)dy_0}{y_0 - y} = -W_{zy}(y) \quad (11)$$

and, once $\tilde{H}_y^A$ is found, we easily obtain

$$\tilde{H}_z(y) = W_{zy}(y)[1 + \tilde{H}_y^A(y)]. \quad (12)$$

Returning to (8) and (9), we find the asymptotic behavior of the functions $h_y(y, M_0)$ and $h_z(y, M_0)$ at $|y - y_0| \longrightarrow \infty$, starting with the function $h_y(y, M_0)$. At large values of $|y - y_0|$, harmonics with low spatial frequencies λ make the major contribution to the expansion of (8). Expanding $U(\lambda, z = 0, z_0)$ in powers of small λ, we have

$$U(\lambda, z = 0, z_0) = U(\lambda = 0, z = 0, z_0) + \lambda\frac{dU(\lambda, z = 0, z_0)}{d\lambda}\bigg|_{\lambda = 0} + \ldots;$$

substituting this series into (8) and integrating, we obtain

$$h_y(y, M_0) = \frac{i}{\omega\mu_0}\frac{U(\lambda = 0, z = 0, z_0)}{(y - y_0)^2} + O\left(\frac{1}{(y - y_0)^4}\right). \quad (13)$$

In a similar way, we obtain

$$h_z(y, M_0) = \frac{2i}{\omega\mu_0}\frac{1}{(y - y_0)^3}\frac{dU(\lambda, z = 0, z_0)}{d\lambda}\bigg|_{\lambda = 0} + O\left(\frac{1}{(y - y_0)^5}\right). \quad (14)$$

In order to write the relationship between $\tilde{H}_y^A$ and $\tilde{H}_z$ in the form containing the magnetotelluric impedance, we introduce the functions

$$V_y(z) = U(\lambda = 0, z, z_0),$$
$$V_z(z) = \frac{dU(\lambda, z, z_0)}{d\lambda}\bigg|_{\lambda = 0}. \quad (15)$$

The function $V_y(z)$ is the solution of problem (10) at $\lambda = 0$. Equations enabling the determination of the function $V_z(z)$ are obtained by differentiating (10) with respect to λ and setting $\lambda = 0$:

$$\frac{d^2V_z(z)}{dz^2} + i\omega\mu_0\sigma(z)V_z(z) = 0, \quad z \in [0, H],$$
$$\frac{\partial V_z(z)}{dz}\bigg|_{z = +0} = -V_y(0), \quad (16)$$
$$\frac{\partial V_z(z)}{dz}\bigg|_{z = H} - \sqrt{-i\omega\mu_0\sigma_H}V_z(H) = 0.$$

In this notation, we have

$$h_y(y, M_0) = \frac{i}{\omega\mu_0}\frac{V_y(0)}{(y - y_0)^2} + O\left(\frac{1}{(y - y_0)^4}\right),$$
$$h_z(y, M_0) = \frac{2i}{\omega\mu_0}\frac{V_z(0)}{(y - y_0)^3} + O\left(\frac{1}{(y - y_0)^5}\right). \quad (17)$$

Returning to (7), we determine the asymptotic behavior of the anomalous magnetic field at $|y - y_0| \longrightarrow \infty$:

$$\tilde{H}_y^A(y) = \frac{i}{\omega\mu_0}V_y(0)\int_S\frac{j_x(M_0)}{(y - y_0)^2}dS = \frac{i}{\omega\mu_0}\frac{V_y(0)}{(y - y_S)^2} \times \int_S j_x(M_0)dS = \frac{i}{\omega\mu_0}\frac{V_y(0)}{(y - y_S)^2}J_x,$$
$$\tilde{H}_z(y) = \frac{2i}{\omega\mu_0}V_z(0)\int_S\frac{j_x(M_0)}{(y - y_0)^3}dS = \frac{2i}{\omega\mu_0}\frac{V_z(0)}{(y - y_S)^3} \times \int_S j_x(M_0)dS = \frac{2i}{\omega\mu_0}\frac{V_z(0)}{(y - y_S)^3}J_x, \quad (18)$$

where

$$J_x = \int_S j_x(M_0)dS$$

is the total excess current in the inhomogeneity and y_S is the coordinate of a point in the central part of its cross section S. Thus, according to (16), we have

$$\frac{\tilde{H}_z(y)}{\tilde{H}_y^A(y)} = \frac{2}{(y - y_S)}\frac{V_z(0)}{V_y(0)} = -\frac{2}{(y - y_S)}\frac{V_z(0)}{\dfrac{dV_z(z)}{dz}\Big|_{z = 0}} \quad (19)$$

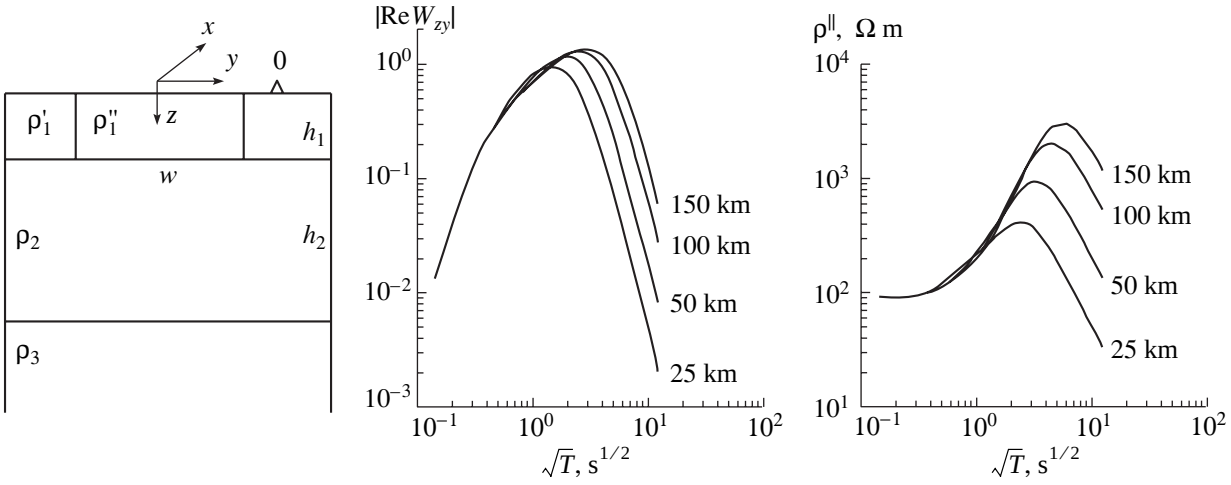

Fig. 3. Model illustrating MVS sensitivity to variations in the normal structure: $\rho_1' = 100\ \Omega$ m; $\rho_1'' = 10\ \Omega$ m; $\rho_2 = 10\,000\ \Omega$ m; $\rho_3 = 0$; $h_1 = 1$ km; $h_2 = 24$, 49, 99, and 149 km. The parameter of the curves is $H = h_1 + h_2$.

in a region located sufficiently far from the inhomogeneity S ($|(y - y_S)| \gg d$).

In order to show that the ratio $\tilde{H}_z/\tilde{H}_y^A$ can be expressed through the normal impedance of the Earth, we introduce the function

$$Z(z) = i\omega\mu_0 \frac{V_z(z)}{\dfrac{dV_z(z)}{dz}}. \qquad (20)$$

According to (16), this function satisfies the Riccati equation

$$\frac{dZ(z)}{dz} - \sigma_N(z)Z^2(z) = i\omega\mu_0 \qquad (21)$$

with the boundary condition

$$Z(H) = \sqrt{\frac{-i\omega\mu_0}{\sigma_H}}. \qquad (22)$$

We obtained the well-known problem for the impedance of a 1-D medium with the conductivity $\sigma_N(z)$ [Berdichevsky and Dmitriev, 1991, 2002]. In the model under consideration, the function $Z(z)$ is evidently the normal impedance of the Earth $Z_N(z)$. Setting $Z(z) = Z_N(z)$ and taking (19)–(22) into account, we find the far-zone asymptotics

$$Z_N(0) = -\frac{i\omega\mu_0(y - y_S)}{2} \frac{\tilde{H}_z(y)}{\tilde{H}_y^A(y)}\bigg|_{|y - y_S| \gg d}, \qquad (23)$$

which coincides with the known expression for the far field of an infinitely long linear current [Vanyan, 1965]. The normal impedance Z_N is connected with the ratio of the components $\tilde{H}_z$ and $\tilde{H}_y^A$ of the anomalous magnetic field, which can be found, according to (11) and (12), from values of the tipper W_{zy} specified at all points of the y axis $(-\infty, \infty)$. If the tipper W_{zy} is given all along the y axis, we synthesize the anomalous magnetic field $(\tilde{H}_z, \tilde{H}_y^A)$ and calculate the normal impedance from the far-zone asymptotics. Knowing the anomalous magnetic field $(\tilde{H}_z, \tilde{H}_y^A)$ and the normal impedance Z_N, we integrate the second equation of Maxwell (the Faraday law) and extend the longitudinal impedance $Z^{\|}$ to the entire y axis:

$$Z^{\|}(y) = \frac{E_x(y)}{H_y(y)} = \frac{1}{1 + \tilde{H}_y^A}\left\{ Z_N - i\omega\mu_0 \int_{-\infty}^{y} \tilde{H}_z(y)dy \right\}. \qquad (24)$$

Thus, the values of $Z^{\|}$ are found from the values of W_{zy}. A one-to-one correspondence exists between the distribution of W_{zy} and $Z^{\|}$. Consequently, we can apply the theorem of Gusarov [1981], stating that the $Z^{\|}$ inversion has a unique solution, and extend this result to the W_{zy} inversion. The uniqueness theorem for the 2-D MVS inversion reduces to that for the 2-D magnetotelluric inversion of the TE-mode. Both methods, MVS and MTS, have a common mathematical basis. A distribution of electrical conductivity is uniquely determined by exact values of impedances or tippers specified at all

points of the Earth's surface for the entire range of frequencies.

A similar approach reducing the uniqueness theorem for the tipper to that for the impedance tensor can prove useful for the analysis of the 3-D MVS problem.

Finally, we consider a model illustrating the sensitivity of the tipper to variations in the normal section (Fig. 3). This three-layer model ($\rho_1 = 100\ \Omega$ m, $\rho_2 = 10\,000\ \Omega$ m, and $\rho_3 = 0$; $h_1 = 1$ km and $h_2 = 24$, 49, 99, and 149 km) contains a near-surface rectangular inclusion 16 km in width with the resistivity $\rho_1' = 10\ \Omega$ m. Observations are conducted at a point O at a distance of 1 km from the inclusion edge. The frequency responses of the tipper clearly reflect the variations in the depth ($H = h_1 + h_2$) to the conducting basement. It is noteworthy that the curves of the real tipper $|\mathrm{Re}\, W_{zy}|$ and longitudinal apparent resistivity $\rho^{\parallel}$ have similar bell shapes. However, the curves $|\mathrm{Re}\, W_{zy}|$ are somewhat less sensitive to variations in H than the curves $\rho^{\parallel}$.

MODEL EXPERIMENTS ON THE 2-D INTEGRATED INTERPRETATION OF MVS AND MTS DATA

The inverse problem of electromagnetic sounding using the magnetotelluric field consists in the determination of the Earth's electrical conductivity from the dependence of components of the tipper and impedance tensor on the position of the observation point and the frequency of field variations. This problem is unstable and therefore ill-posed [Dmitriev, 1987; Berdichevsky and Dmitriev, 1991, 2002]. An arbitrarily small error in field characteristics can give rise to an arbitrarily large error in the conductivity distribution. The solution of such a problem is meaningful if, using a priori information on the structure of the medium studied, one limits the region of parameters to be found, and an approximate solution of the inverse problem is sought within a compact set of plausible models forming an interpretation model.

A geoelectric interpretation model should reflect current notions and hypotheses on the sedimentary cover, crust, and upper mantle. Depending on the amount of a priori information, the goal of research, and the field characteristics used, the model can either smooth or emphasize geoelectric contrasts and incorporate inhomogeneous layers and local inclusions of higher or lower electrical conductivity. An approximate solution of an inverse problem constrained by the interpretation model is chosen using criteria ensuring the agreement of the solution with the available a priori information and pertinent characteristics of the field (the criteria of the a priori information significance and model misfit). This approach was implemented in the regularized optimization method [Dmitriev, 1987; Berdichevsky and Dmitriev, 1991, 2002]. The number of such criteria is determined by the number of characteristics specifying the field (real, imaginary, amplitude, and phase characteristics). If the inversion uses a few characteristics of the field, the problem is multicriterion.

The 2-D integrated interpretation of MVS and MTS data belongs to the class of multicriterion problems. The determination of the electrical conductivity of the Earth requires data on the TE-mode with the characteristics $\mathrm{Re}\, W_{zy}$, $\mathrm{Im}\, W_{zy}$, $\rho^{\parallel}$, and $\varphi^{\parallel}$ (real and imaginary tippers, longitudinal apparent resistivities, and phases of longitudinal impedances) and on the TM-mode with the characteristics $\rho^{\perp}$ and $\varphi^{\perp}$ (transverse apparent resistivities and phases of transverse impedances). These parameters differ in sensitivity to target geoelectric structures and in stability with respect to near-surface distortions [Berdichevsky and Dmitriev, 2002]. The TE-mode is more sensitive to deep conducting structures and less sensitive to the resistance of the lithosphere, whereas the TM-mode is less sensitive to deep conducting structures and more sensitive to the resistance of the lithosphere. In addition, note that apparent resistivities in the entire range of low frequencies can be subjected to strong static distortions due to local 3-D near-surface inhomogeneities (geoelectric noise), whereas low-frequency tippers and impedance phases are free from these distortions. An algorithm of the 2-D bimodal inversion should implement a procedure in which the field characteristics in use support and complement each other: gaps arising in the inversion of one characteristic of the field should be filled through the inversion of another. In inverting various field characteristics, one should give priority to the most reliable elements of the model and suppress the least reliable ones.

The following two approaches are possible in solving multicriterion inverse problems: (i) parallel (joint) inversion of all field characteristics used and (ii) successive (partial) inversions of each of the field characteristics.

The parallel inversion summarizes all inversion criteria related to various field characteristics and reduces in a 2-D variant to the minimization of the Tikhonov's functional

$$\inf_{\mathbf{p}}\left\{\sum_{m=1}^{M}\gamma_m\left\|F_m(y,\omega)-I_m(\sigma)\right\|^2+\alpha\Omega(\sigma)\right\}, \qquad (25)$$

where the following notation is used: $\mathbf{p}$, vector of the sought-for parameters; F_m, field characteristic in use; y, coordinate of the observation point; ω, frequency; I_m, operator determining F_m from the known distribution of the conductivity σ; γ_m, significance coefficient of the criterion of the model misfit (the deviation I_m from F_m); Ω, solution selection criterion (stabilizer) adjusting the solution to the a priori information; α, regularization parameter (the significance coefficient of the a priori information); M, number of the field characteristics used.

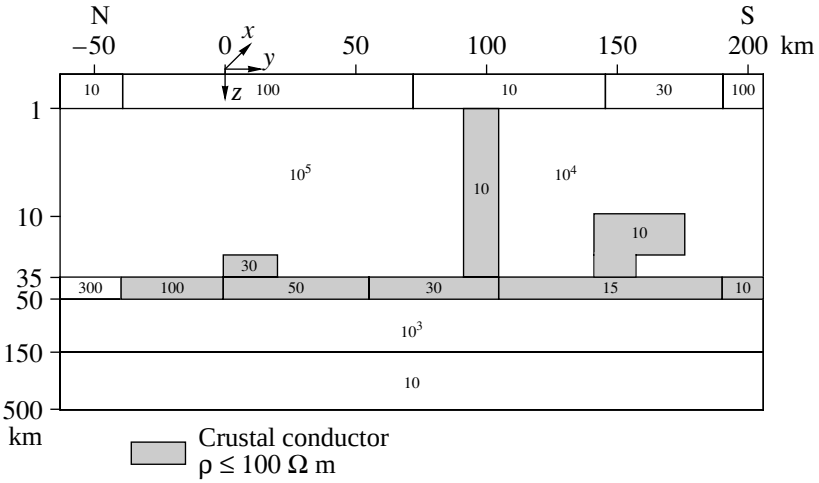

Fig. 4. The 2-D TS model. The zone of lower crustal resistivities is shaded, and resistivity values (in Ω m) are shown within blocks.

At first glance, the parallel inversion seems to be the most effective because it incorporates simultaneously all specific features of the multicriterion problem and significantly simplifies the work of the geophysicist. However, this approach is open to criticism.

If various characteristics F_m have the same sensitivity to all parameters $\mathbf{p}(p_1, p_2, \ldots, p_s)$ of the geoelectric structure, their parallel inversion is not very advantageous because one, the most reliably determined, characteristic is sufficient for a comprehensive inversion.

The use of several characteristics of the field makes the inversion more informative if they differ significantly in their sensitivity to various parameters of the geoelectric structure. However, in this case their joint inversion can become conflicting, because they provide different constraints on the geoelectric structure and are related to different criteria of model misfits and solution selection. It is possible that in some cases a fortunate selection of weights allows one to construct a self-consistent model with a small overall misfit. However, the reasonable selection of such weights is itself a complex problem that often cannot be solved as yet. Apparently, a succession of partial inversions is the best approach to the solution of a multicriterion inverse problem.

Let a field characteristic F_m be the most sensitive to the vector of parameters $\mathbf{p}^{(m)}$. Then, the partial mth inversion of the multicriterion 2-D problem consists in the minimization of the following Tikhonov's functional on the set of the parameters $\mathbf{p}^{(m)}$, with the parameters $\mathbf{p} - \mathbf{p}^{(m)}$ being fixed:

$$\inf_{\mathbf{p}^{(m)}} \{ \| F_m(y, \omega) - I_m(\sigma) \|^2 + \alpha\Omega(\sigma) \}. \qquad (26)$$

The successive application of the field characteristics F_m ($m = 1, 2, \ldots, M$) reduces the solution of the multicriterion problem to a succession of partial inversions. Each partial inversion is intended for the solution of a specific problem and can be restricted to specific structures.

A decrease in the number of parameters minimizing the Tikhonov's functional significantly enhances the stability of the problem. Partial inversions comprehensively incorporate specific features of the field characteristics used, their informativeness, and their confidence intervals. They admit information exchange between various field characteristics, enable a convenient interactive dialog, and are easily tested. We believe that this direction of research is most promising for further development of methods designed for the integrated interpretation of MVS and MTS data.

The method of partial inversions is corroborated by results of studies carried out in various geological provinces [Trapeznikov *et al.*, 1997; Berdichevsky *et al.*, 1998, 1999; Pous *et al.*, 2001; Vanyan *et al.*, 2002]. Below, we describe model experiments performed by this method.

Figure 4 presents a 2-D model schematically illustrating geoelectric structure of the Kyrgyz Tien Shan [Trapeznikov *et al.*, 1997]. This model, referred to below as the TS model, includes the following elements: (1) an inhomogeneous sedimentary cover whose resistivity ranges from 10 to 100 Ω m; (2) an inhomogeneous upper crust with a resistivity of 10^5 Ω m in the north and 10^4 Ω m in the south; (3) an inhomogeneous conducting layer in the lower crust (35–50 km) resistivity in which increases monotonically from 10 Ω m in the south to 300 Ω m in the north; (4) homogeneous conducting zones A, B, and C branching from the crustal conducting layer (they are regarded as fault

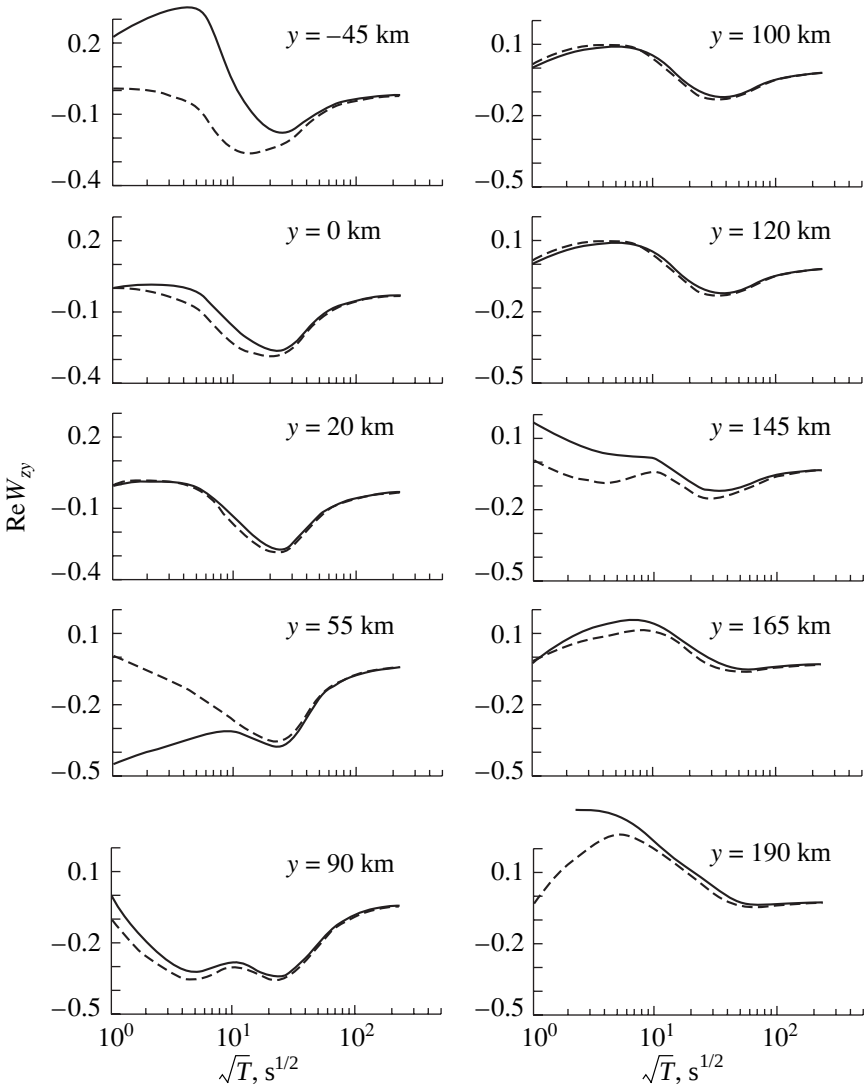

Fig. 5. Frequency responses of $\mathrm{Re}\,W_{zy}$. Solid and broken lines are the TS models with inhomogeneous and homogeneous upper layers, respectively.

zones); and (5) a homogeneous, poorly conducting mantle (10^3 Ω m) underlain by a conducting mantle (10 Ω m) at a depth of 150 km. The model is excited by a vertically incident plane wave.

The forward problem was solved with the use of a program implementing the finite element method [Wannamaker *et al.*, 1987]. Gaussian white noise was introduced into the resulting field characteristics; the noise had standard deviations of 5% for longitudinal and transverse apparent resistivities $\rho^{\parallel}$ and $\rho^{\perp}$, 2.5° for phases of longitudinal and transverse impedances $\varphi^{\parallel}$ and $\varphi^{\perp}$, and 5% for real and imaginary parts of the tipper $\mathrm{Re}\,W_{zy}$ and $\mathrm{Im}\,W_{zy}$. To imitate the static shift due to small near-surface (3-D) inhomogeneities, the apparent resistivity curves were multiplied by random real numbers uniformly distributed in the interval from 0.5 to 2.

It is of interest to estimate the frequency interval within which the tipper is unaffected by the upper layer inhomogeneities. Figures 5 and 6 present the frequency responses of $\mathrm{Re}\,W_{zy}$ and $\mathrm{Im}\,W_{zy}$ calculated for the TS model and for the same model with a homogeneous upper layer of a resistivity of 10 Ω m. Except for a few points (y = 45 km for $\mathrm{Re}\,W_{zy}$ and y = –45, 55, and 100 km for $\mathrm{Im}\,W_{zy}$), the $\mathrm{Re}\,W_{zy}$ and $\mathrm{Im}\,W_{zy}$ curves calculated for the TS models with inhomogeneous and homogeneous upper layers coincide at periods of about 100 s and even less. These are periods of the low-frequency interval, in which the MVS near-surface effects attenuate and the effects of crustal inhomogeneities become appreciable.

The integrated interpretation of the synthetic characteristics of the field obtained from the TS model was performed by the method of partial inversions.

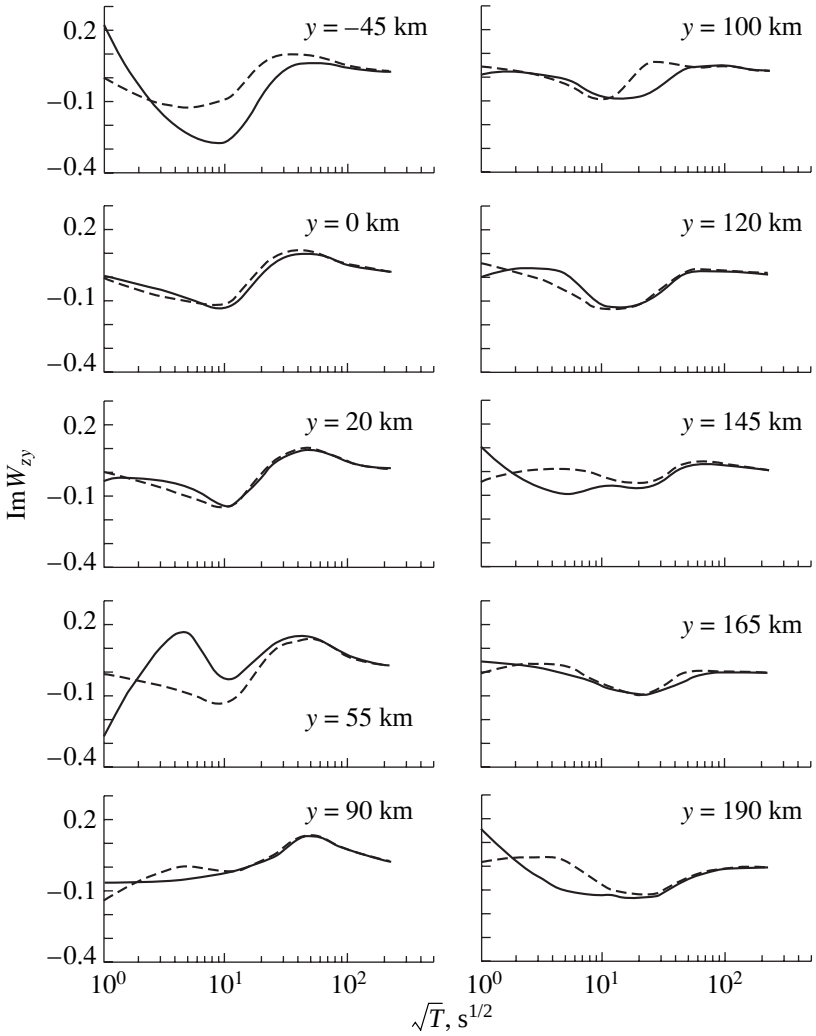

Fig. 6. Frequency responses of Im W_{zy}. Solid and broken lines are the TS models with inhomogeneous and homogeneous upper layers, respectively.

The construction of the interpretation model is the most important stage of an interpretation [Dmitriev, 1987; Berdichevsky and Dmitriev, 1991, 2002]. The interpretation model should meet the following two requirements: it should be informative (i.e., reflect the main features of the study section, including target layers and structures) and it should be simple (i.e., be determined by a small number of parameters ensuring the stability of the inverse problem).

It is evident that these requirements are antagonistic: a more informative model is more complex. Therefore, an optimal model, both simple and informative enough, should be chosen. This is a key point of the interpretation, determining both the strategy and even, to an extent, the solution of the inverse problem. The choice of the interpretation model is a matter of the intuition of a researcher and his or her experience, understanding of the real geological situation, adherence to traditions, and ability to depart from traditional approaches. Although the choice of the optimal model is subjective, it is restrained by a priori information, qualitative estimates, and reasonable hypotheses on the structure of the medium studied.

Constructing the interpretation model for inversions of the synthetic TS characteristics of the field, we assumed that the following a priori information on the study medium was available: (1) the sedimentary cover is inhomogeneous, with a tentative thickness of 1 km; (2) the consolidated crust is inhomogeneous and can contain local conducting zones, its resistivity can experience regional variations, and an inhomogeneous conducting layer corresponding to the seismic waveguide possibly exists in its lower part at depths of 35 to 50 km; and (3) the upper mantle consists of homogeneous layers, and its resistivity at depths below 200 km can amount to a few tens of ohm meter units.

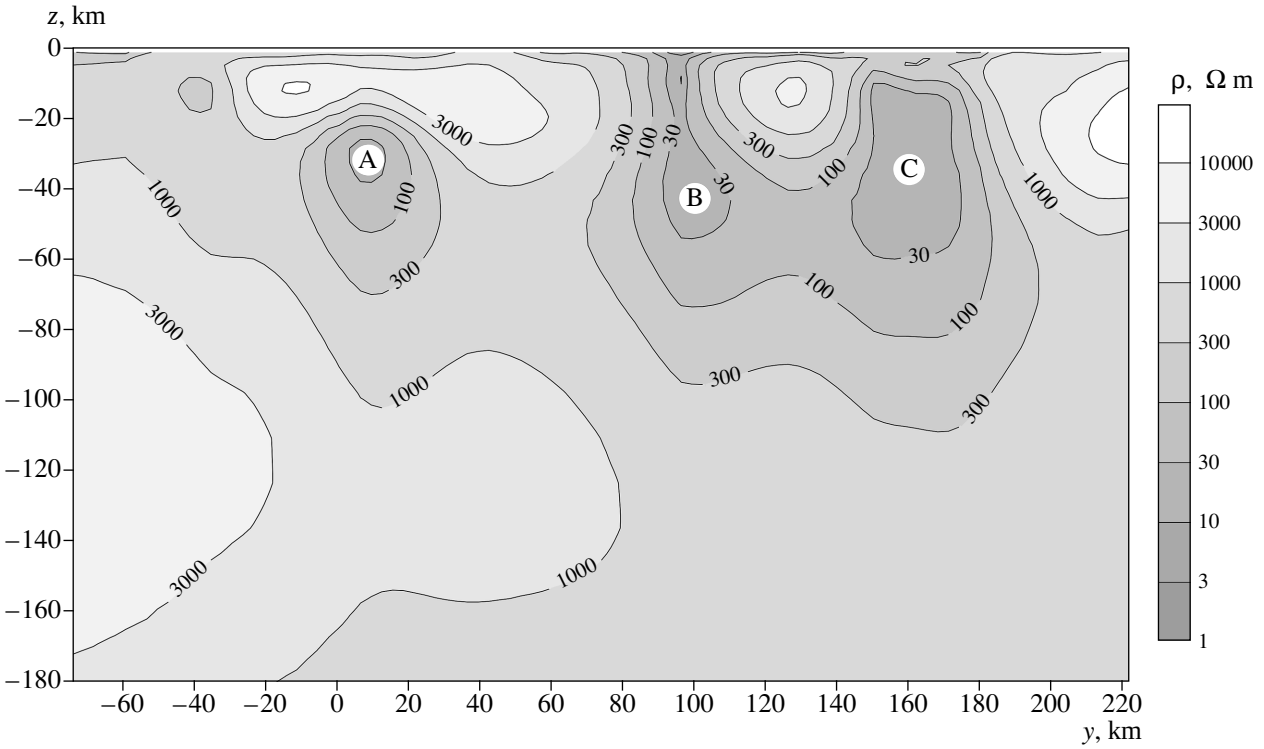

Fig. 7. The TP-1 model: inversion of $\mathrm{Re}\, W_{zy}$ and $\mathrm{Im}\, W_{zy}$ using the REBOCC program; A, B, and C are conducting zones in the crust (cf. Fig. 4).

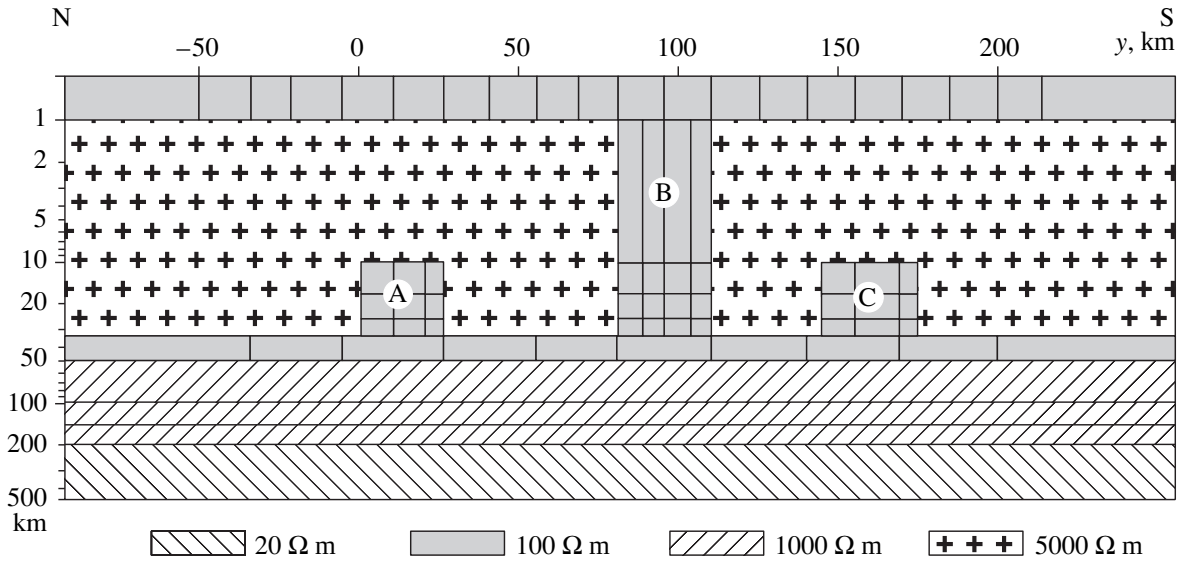

Fig. 8. The interpretation block model for successive partial inversions; starting values of resistivities (in Ω m) are shown within blocks.

To additionally refine this information, we inverted the tippers using a smoothing program capable of identifying and localizing crustal conductors. We applied the REBOCC program [Siripunvaraporn and Egbert, 2000] using, as an initial approximation, a homogeneous half-space with a resistivity of 100 Ω m. Figure 7 presents the TP-1 model, resulting from the inversion of $\mathrm{Re}\, W_{zy}$ and $\mathrm{Im}\, W_{zy}$. This model yields clear evidence of three local crustal conducting zones A, B, and C ($\rho < 30$ Ω m) but fails to distinctly resolve layers in the crust and upper mantle.

The a priori information complemented with data on local crustal conductors provides a reasonable basis for

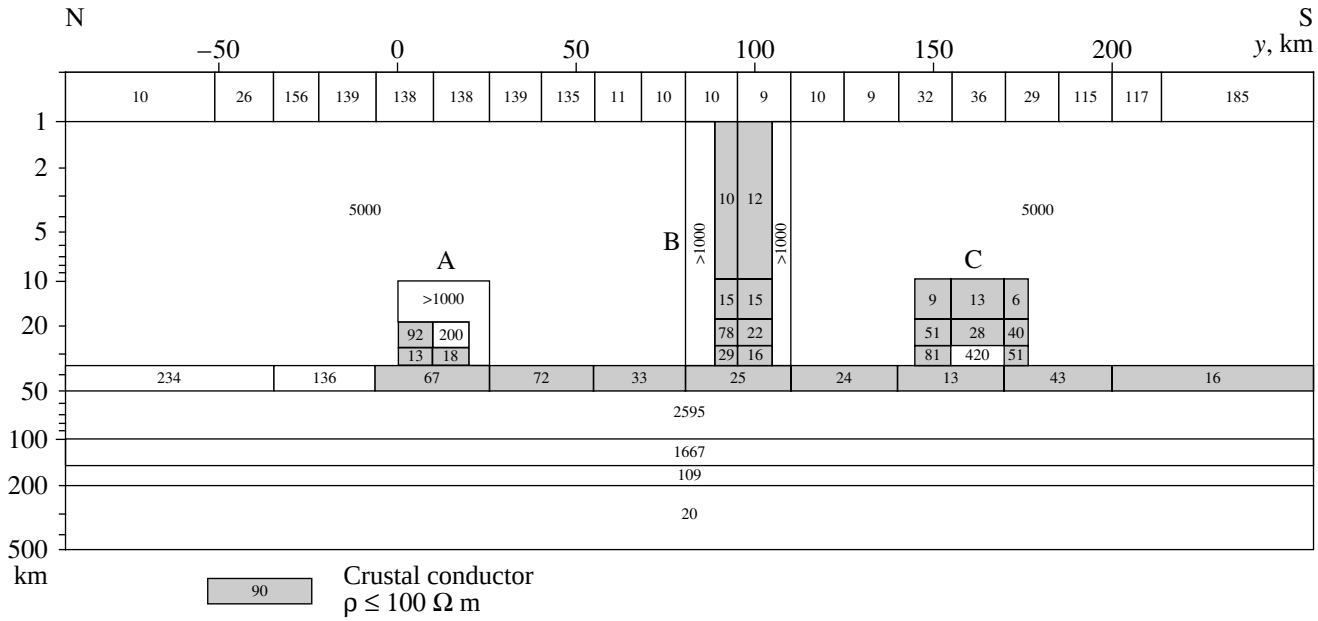

Fig. 9. The TP-2 model: inversion of $\mathrm{Re}\,W_{zy}$ and $\mathrm{Im}\,W_{zy}$ using the II2DC program; resistivity values (in Ω m) are shown within blocks, and the region of lower crustal resistivities is shaded (cf. Fig. 4).

the construction of a block interpretation model. This model, presented in Fig. 8, consists of 70 blocks of a fixed geometry. The concentration of blocks depends on the position and size of tentative structures and is highest within the sedimentary cover, local crustal conductors, and crustal conducting layer. In minimizing Tikhonov's functional, resistivities of the blocks are varied. The starting values of resistivities are shown in the model presented in Fig. 8.

Partial inversions of the synthetic characteristics of the field were performed in the class of block structures with the use of the II2DC program [Varentsov, 2002] in the following succession: (1) $\mathrm{Re}\,W_{zy}$ and $\mathrm{Im}\,W_{zy}$ inversion $\longrightarrow$ (2) $\varphi^{\parallel}$ inversion $\longrightarrow$ (3) $\rho^{\perp}$ and $\varphi^{\perp}$ inversion. All the inversions were conducted automatically. Below, we consider each inversion separately.

1. Inversion of $\mathrm{Re}\,W_{zy}$ and $\mathrm{Im}\,W_{zy}$. The starting model is shown in Fig. 8. Due to the absence of near-surface distortions, the tipper inversion can provide reliable constraints on main structures of the medium studied. As a result, we obtained the TP-2 model, shown in Fig. 9, which agrees well with the TS model. The divergence between the tippers calculated from both models is generally no more than 5–7% in the period range from 1 to 10 000 s (Fig. 10). Using the MVS data alone, we successfully reconstructed (in the automatic regime, without any corrections!) the most significant elements of the study section, including the inhomogeneous sedimentary cover; the local crustal conductors A, B, and C; and the inhomogeneous crustal conducting layer whose resistivity varies from 234 Ω m in the north to 16 Ω m in the south (from 300 to 10 Ω m in the initial model). Also resolved was the contrast between the nonconductive and conductive mantle (1667 Ω m/109 Ω m in the TP-2 model and 1000 Ω m/10 Ω m in the initial TS model). We see that the MVS characteristics of the field measured on a 200-km profile allowed us not only to detect the local conducting zones but also to determine the stratification of the section (with an accuracy sufficient for obtaining gross petrophysical estimates).

2. Inversion of $\varphi^{\parallel}$. At this stage, without going beyond the TE-mode, we control the tipper inversion and gain additional constraints on the stratification of the section. A difficulty consists in the fact that the curves of the longitudinal apparent resistivity $\rho^{\parallel}$ are distorted by near-surface 3-D inhomogeneities that create geoelectric noise and need to be allowed for. We avoided this difficulty by restricting ourselves to the inversion of the undistorted curves $\varphi^{\parallel}$. If $\rho^{\parallel}$ and $\varphi^{\parallel}$ are interrelated through dispersion relations, the disregard of the curves $\rho^{\parallel}$ does not lead to a loss of information. We interpreted the curves $\varphi^{\parallel}$ using as a starting model the TP-2 model, obtained from the tipper inversion. We remind the reader that phase inversion gives a resistivity distribution accurate to an unknown scalar factor (as is evident from the analysis of 1-D models). To eliminate this uncertainty, we fixed the resistivities of the sedimentary cover and the upper nonconductive crust. Figure 11 presents the TE model, obtained from the phase inversion. The divergences between the phases calculated from the TE and initial TS models do not exceed 2.5° (Fig. 12). Comparing the TE and TP-2 models, we see that the phase inversion agrees reasonably well with the tipper inversion. Two points are of particular interest here: (1) the boundary resistivities of

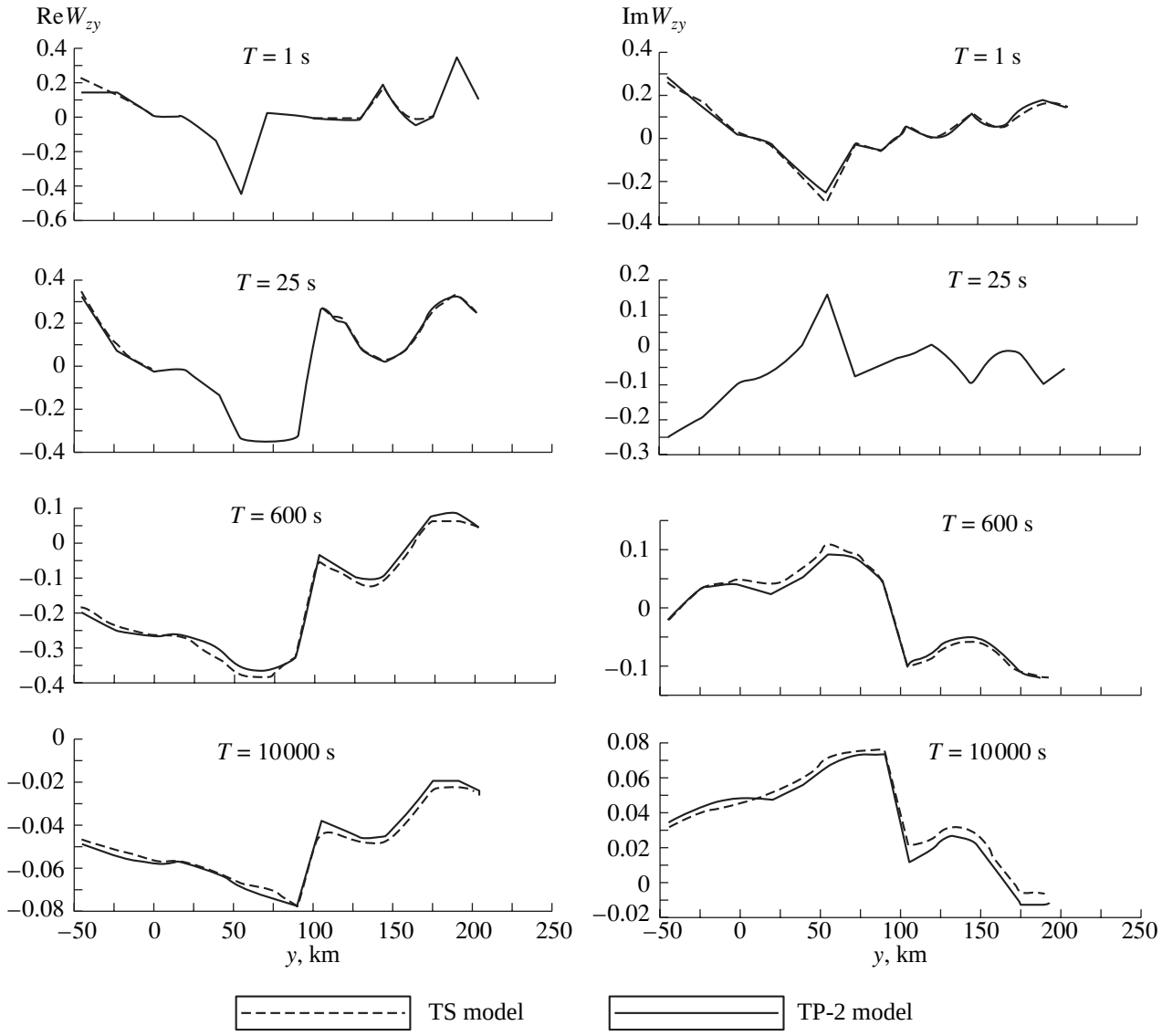

Fig. 10. Comparison of frequency responses of $\mathrm{Re}\,W_{zy}$ and $\mathrm{Im}\,W_{zy}$ calculated from the TS and TP-2 models.

the inhomogeneous crustal layer (343 and 10 Ω m) became closer to their true values (300 and 10 Ω m), and (2) the contrast between the nonconductive and conductive mantle became sharper (3801 Ω m/15 Ω m in the TE model versus 1000 Ω m/10 Ω m in the initial TS model). Thus, phase inversion significantly improves the accuracy of the section stratification.

3. Inversion of $\rho^{\perp}$ and $\varphi^{\perp}$. This inversion is intended for estimating the resistivity of the upper, highly resistive crust ρ_{upper}. The TE model, obtained from the $\varphi^{\parallel}$ inversion, was used as a starting model. Focusing the inversion of $\rho^{\perp}$ and $\varphi^{\perp}$ on the upper crust, we fixed all resistivities except for ρ_{upper}. As a result, the inversion of $\rho^{\perp}$ and $\varphi^{\perp}$ yielded the TM model, shown in Fig. 13. The divergences between the apparent resistivities $\rho^{\perp}$ calculated from the TM and initial TS models are seen from Fig. 14. Both models yield similar regional variations of $\rho^{\perp}$ with a local scatter associated with the geoelectric noise. The phase misfits of the TM model do not exceed 2.5°. The TM model reveals the asymmetry of the highly resistive upper crust: from 283 000 Ω m in the north to 13 000 Ω m in the south (in the initial TS model, from 10^5 Ω m in the north to 10^4 Ω m in the south).

The TM model is the final model obtained from the successively applied automatic partial inversions. Its agreement with the initial TS model is evident (cf. Figs. 13 and 4). All of the major TS structures are well resolved in the TM model. Misfits between these models do not exceed 5–7% in tippers and 2.5° in phases.

For comparison, Fig. 15 presents the PI model, obtained by the parallel (joint) inversion of all charac-

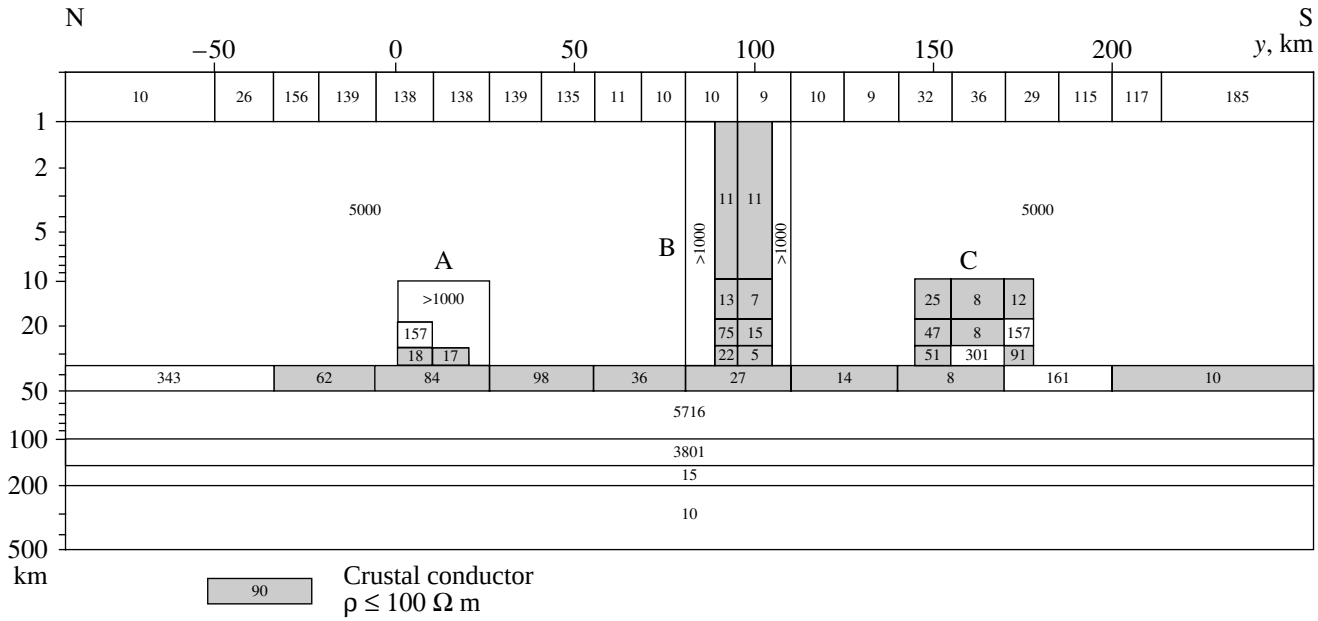

Fig. 11. The TE model: inversion of $\varphi^{\parallel}$ using the II2DC program; resistivity values (in Ω m) are shown within blocks, and the region of lower crustal resistivities is shaded (cf. Fig. 4).

teristics of the field ($\mathrm{Re}\,W_{zy}$, $\mathrm{Im}\,W_{zy}$, $\varphi^{\parallel}$, $\rho^{\perp}$, and $\varphi^{\perp}$) used for the construction of the TM model. The starting model used here was the same as in the tipper inversion (Fig. 8). The following features characterize the PI model: (1) resistivity contrasts in the sedimentary cover are significantly smoothed; (2) the resistivity contrast in the upper, highly resistive crust is also significantly smoothed (86 000 Ω m/44600 Ω m versus 283602 Ω m/13278 Ω m in the TM model and 100000 Ω m/10000 Ω m in the initial TS model); (3) the northern conducting zone A is well resolved, the southern conducting zone C is somewhat less expressed, and the central conducting zone B is strongly distorted (this zone, connecting the sedimentary cover with the crustal conducting layer, is only represented by four conducting blocks); (4) the contrast between the two boundary resistivities in the crustal conducting layer is much lower (120 Ω m/29 Ω m versus 343 Ω m/10 Ω m in the TM model and 300 Ω m/10 Ω m in the initial TS model); and (5) the monotonic decrease of resistivities associated with the nonconductive/conductive mantle transition is disturbed (a poorly conducting layer with a resistivity of 7423 Ω m is present in the conducting mantle). We see that the parallel inversion of all characteristics of the field worsened significantly the interpretation result.

Of course, the parallel inversion of all characteristics of the field is the simplest approach to a multicriterion problem, and apparently this is the reason why it is popular among geophysicists fascinated by the possibility of automatic inversions eliminating the necessity of comprehensive analysis of information. The transition to the technique of successive partial inversions undoubtedly complicates the work of the geophysicist, and this is a possible reason for the objections raised in discussions of inverse multicriterion problems of deep geoelectric studies. However, our experiments on the integrated interpretation of MVS and MTS data indicate that the game, albeit more difficult, is worth the candle.

MVS STUDY OF THE CASCADIAN SUBDUCTION ZONE (EMSLAB EXPERIMENT)

The above scheme of partial inversions of MVS and MTS data was applied to the construction of the geoelectric model for the Cascadian subduction zone [Vanyan *et al.*, 2002]. We used data obtained in 1986–1988 by geophysicists from the United States, Canada, and Mexico on the Pacific North American coast within the framework of the experiment "Electromagnetic Study of the Lithosphere and Asthenosphere beneath the Juan de Fuca Plate" (EMSLAB) [Wannamaker *et al.*, 1989a].

Figure 16 presents a predictive petrological and geothermal model of the Cascadian subduction zone along an E–W profile generalizing modern ideas and hypotheses on the structure of the region and its fluid regime [Romanyuk *et al.*, 2001]. The subducting Juan de Fuca plate originates at an offshore spreading ridge (about 500 km from the coast). In the eastward direction, the profile crosses (1) an abyssal basin with a sedimentary cover 1–2 km thick and a pillow lava layer 1.5–2 km thick; (2) the Coast Range, composed of volcanic-sedimentary rocks; (3) the Willamette River valley, filled with a thick sequence of sediments and basaltic intru-

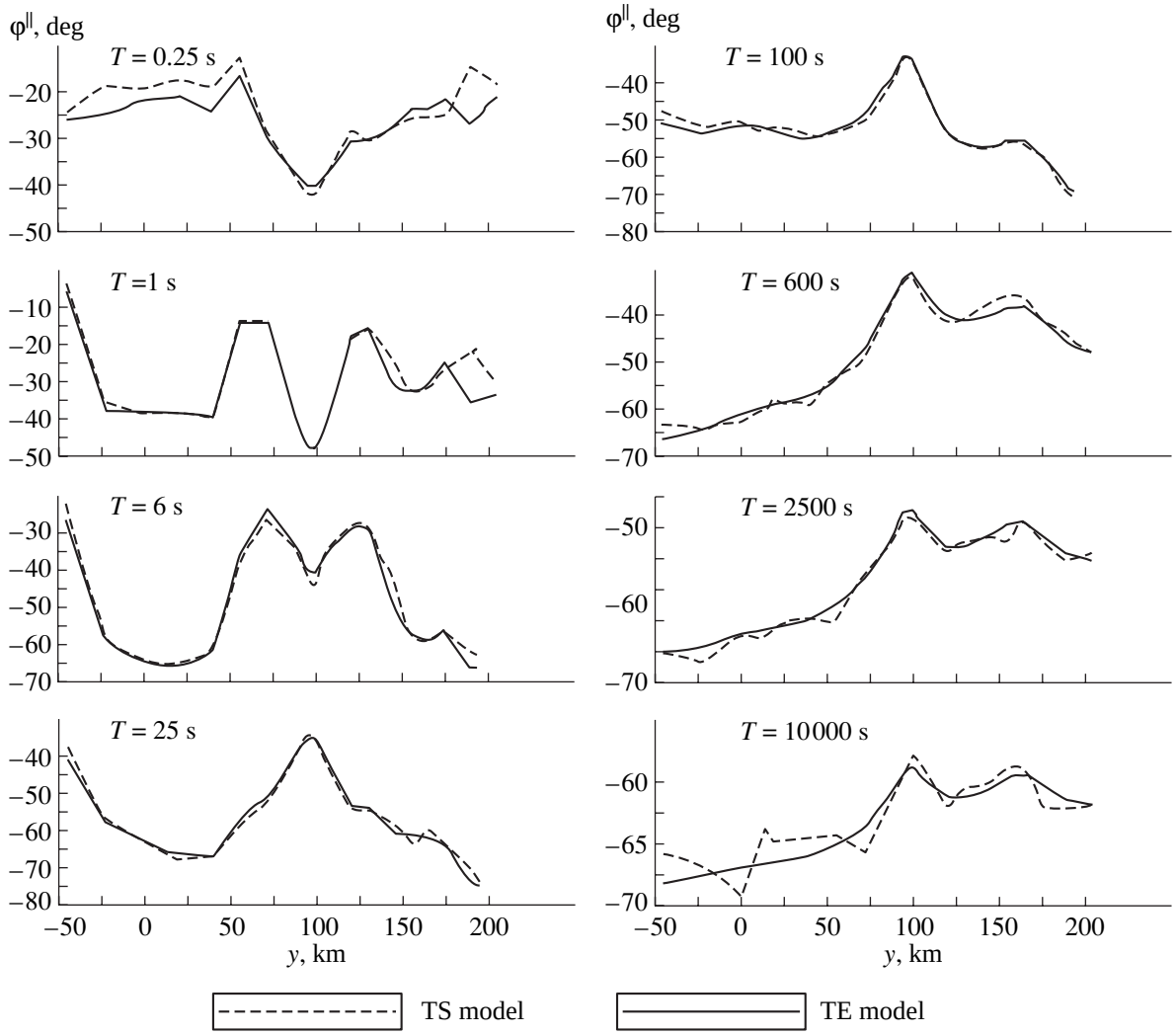

Fig. 12. Comparison of frequency responses of $\varphi^{\parallel}$ calculated from the TS and TE models.

sions; (4) the Western (older) and Eastern (younger) Cascade ranges, consisting of volcanic and volcanic-sedimentary rocks typical of a recent active volcanic arc; and (5) the Deschutes Plateau, covered with lavas.

The abyssal basin is characterized by a typical oceanic section with the asthenosphere at a depth of about 40 km (the 900°C isotherm). The continental crust above the subducting slab has lower temperatures. A subvertical zone of higher temperatures reaching the melting point of wet peridotite (~900°C) has been localized beneath the High Cascades. The release of fluids from the upper part of the slab appears to be due to a few mechanisms. First, at depths to about 30 km, free water is released from micropores and microfractures under the action of the increasing lithostatic pressure. Dehydration of minerals such as talc, serpentine, and chlorite starts at depths of 30 to 50 km, where the temperature exceeds 400°C. Finally the basalt–eclogite transition can start at depths greater than 75 km, and exsolution of amphibolites can take place at depths of more than 90 km. All these processes are accompanied by the release of fluids. Supposedly, fluids released at small depths migrate through the contact zone between the oceanic and continental plates. At greater depths, fluids can be absorbed by mantle peridotites (serpentinization) and, given high temperatures, disturb the equilibrium state of material and give rise to "wet" melting. The melts migrate upward toward the Earth's surface, producing a volcanic arc.

Two 2-D geoelectric models of the Cascadian subduction zone constructed along the Lincoln line (an E–W profile in the middle part of Oregon) have been discussed in literature: EMSLAB-I [Wannamaker *et al.*, 1989b] and EMSLAB-II [Varentsov *et al.*, 1996].

The EMSLAB-I model, shown in Fig. 17a, was constructed by a trial-and-error method with a strong priority given to the TM-mode; the latter, in the opinion of the authors of this model, is least sensitive to deviations

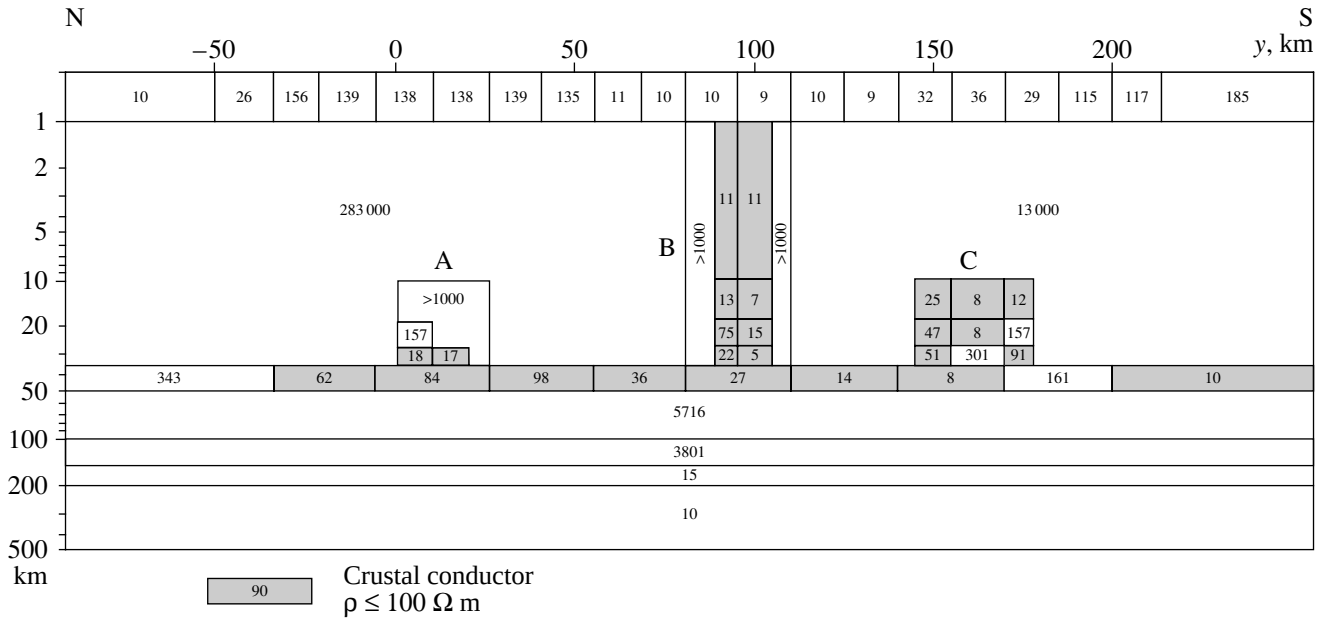

Fig. 13. The TM model: inversion of $\rho^{\perp}$ and $\varphi^{\perp}$ using the II2DC program; resistivity values (in Ω m) are shown within blocks, and the region of lower crustal resistivities is shaded (cf. Fig. 4).

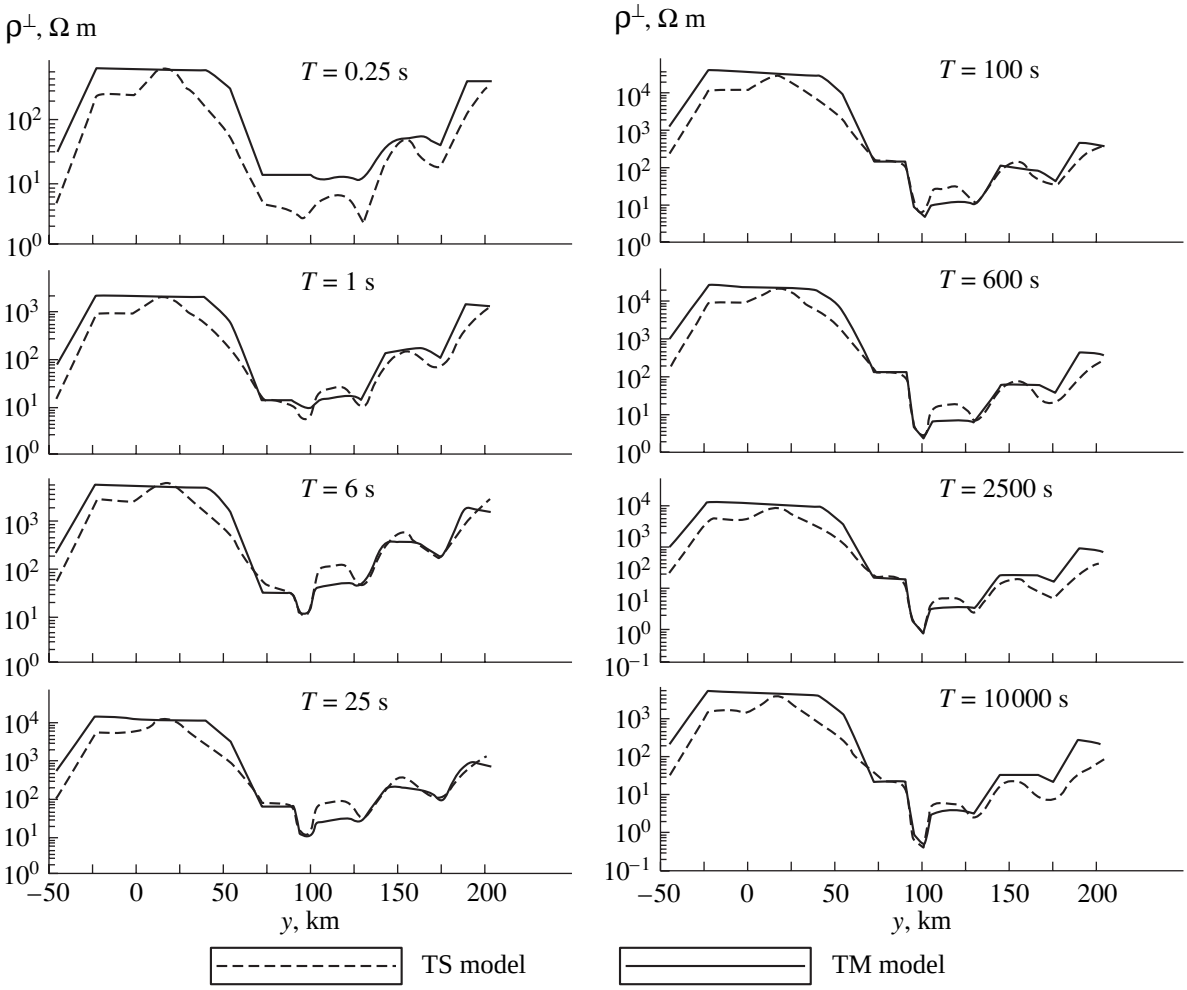

Fig. 14. Comparison of frequency responses of $\rho^{\perp}$ calculated from the TS and TM models.

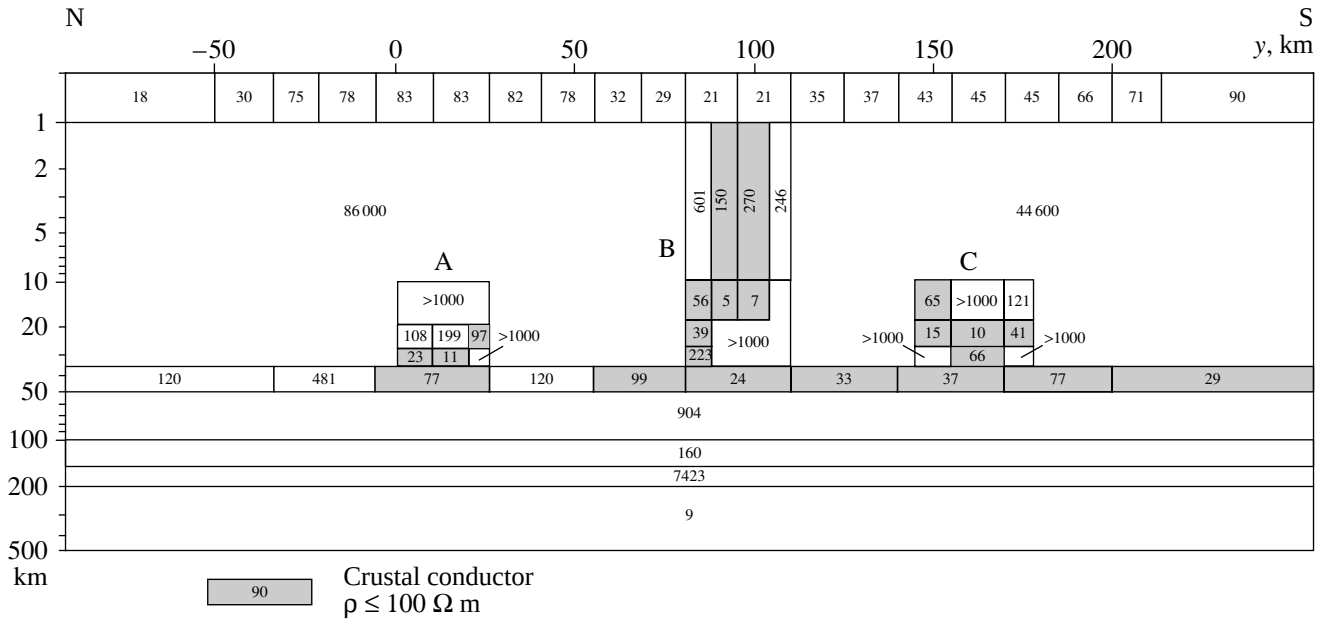

Fig. 15. The PI model: parallel inversion of $\mathrm{Re}\,W_{zy}$, $\mathrm{Im}\,W_{zy}$, $\varphi^{\parallel}$, $\rho^{\perp}$, and $\varphi^{\perp}$ using the II2DC program; resistivity values (in Ω m) are shown within blocks, and the region of lower crustal resistivities is shaded (cf. Fig. 4).

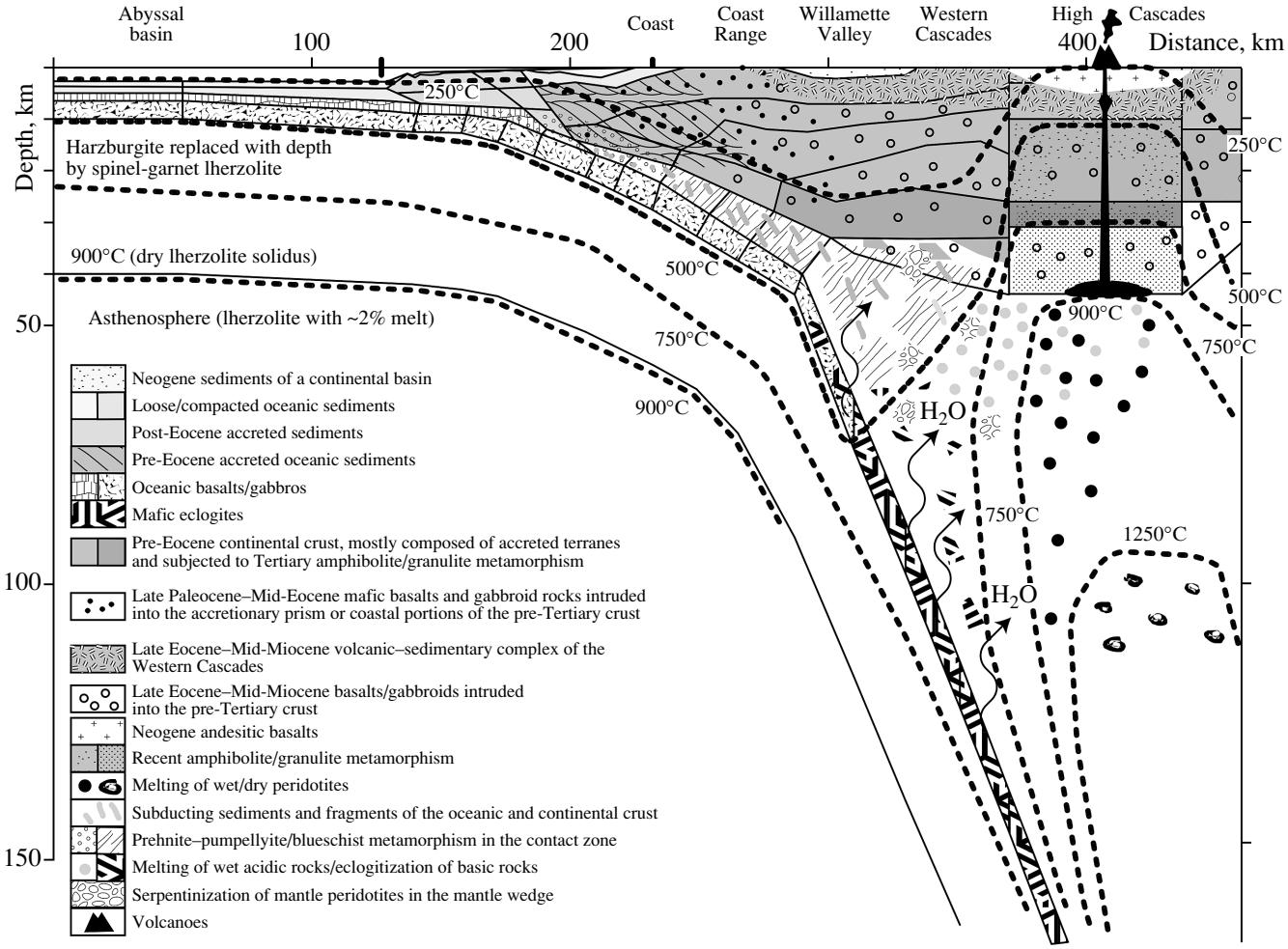

Fig. 16. Predictive geothermal and petrological CASCADIA model, constructed along an E–W profile across central Oregon [Romanyuk *et al.*, 2001].

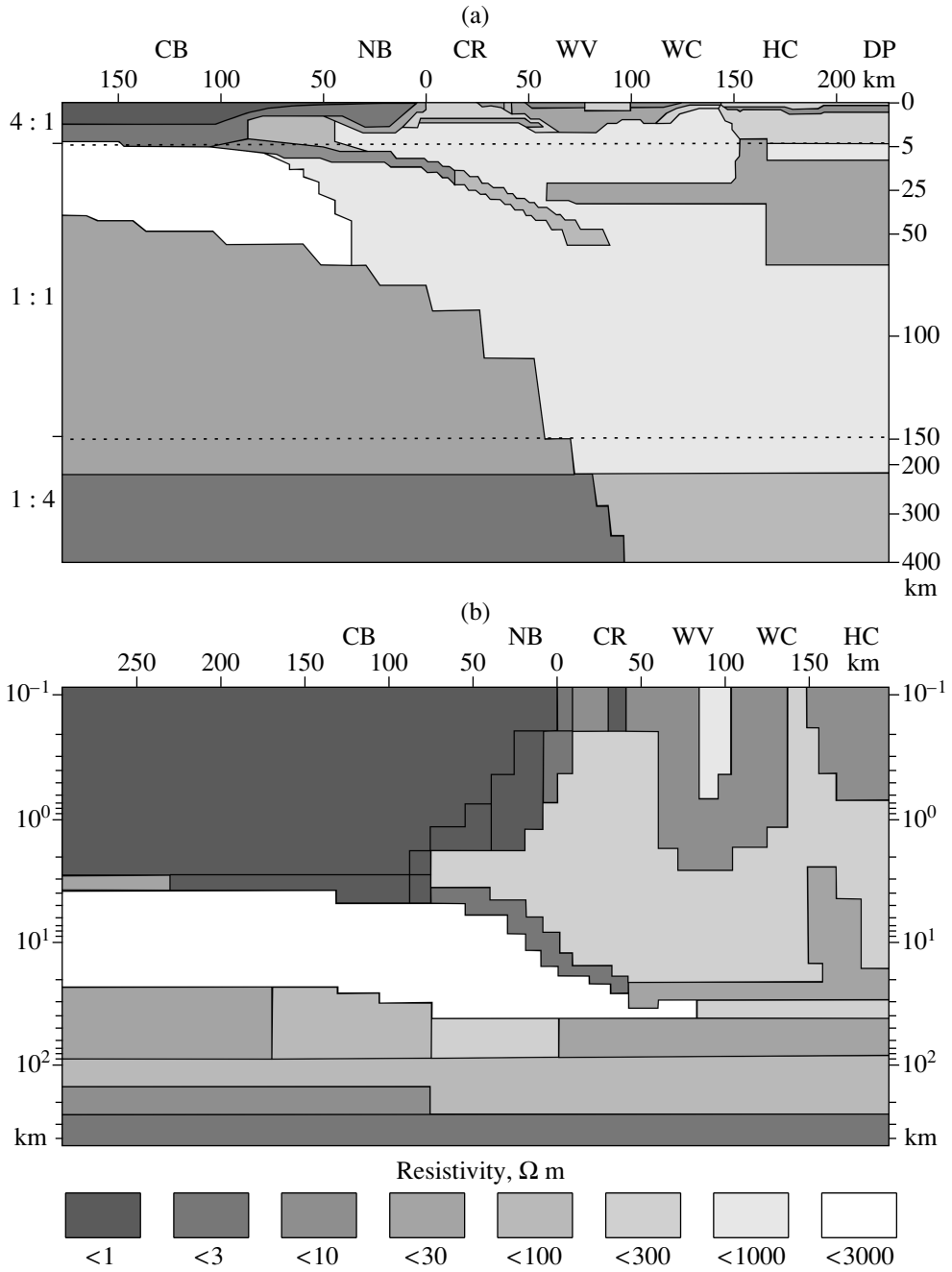

Fig. 17. Geoelectric models of the Cascadian subduction zone: (a) EMSLAB-I [Wannamaker *et al.*, 1989b]; (b) EMSLAB-II [Varentsov *et al.*, 1996]. CB, Cascadia basin; NB, Newport basin; CR, Coast Range; WV, Willamette Valley; WC, Western Cascades; HC, High Cascades; DP, Deschutes Plateau.

from the 2-D pattern. The EMSLAB-I model minimizes the misfits of the curves $\rho^{\perp}$ and $\varphi^{\perp}$ and ignores the curves $\rho^{\parallel}$ and $\varphi^{\parallel}$. Its main elements are (1) the upper conductive part of the plate, sinking at a low angle beneath the Coast Range; (2) a subhorizontal conducting layer in the middle continental crust broadening in the area of the High Cascades; and (3) a well-developed conductive asthenosphere beneath the ocean. The problem of the junction between the slab and the crustal conductor remains open in this model. The continental asthenosphere is not present in this model, although the shape of the experimental curves $\rho^{\parallel}$ and $\varphi^{\parallel}$ suggests a low resistivity of the upper mantle. The absence of large divergences between the model values of $\mathrm{Re}\, W_{zy}$ and $\mathrm{Im}\, W_{zy}$, on the one hand, and the experimental data, on the other hand, is considered by the authors as evidence of the reliability of the model.

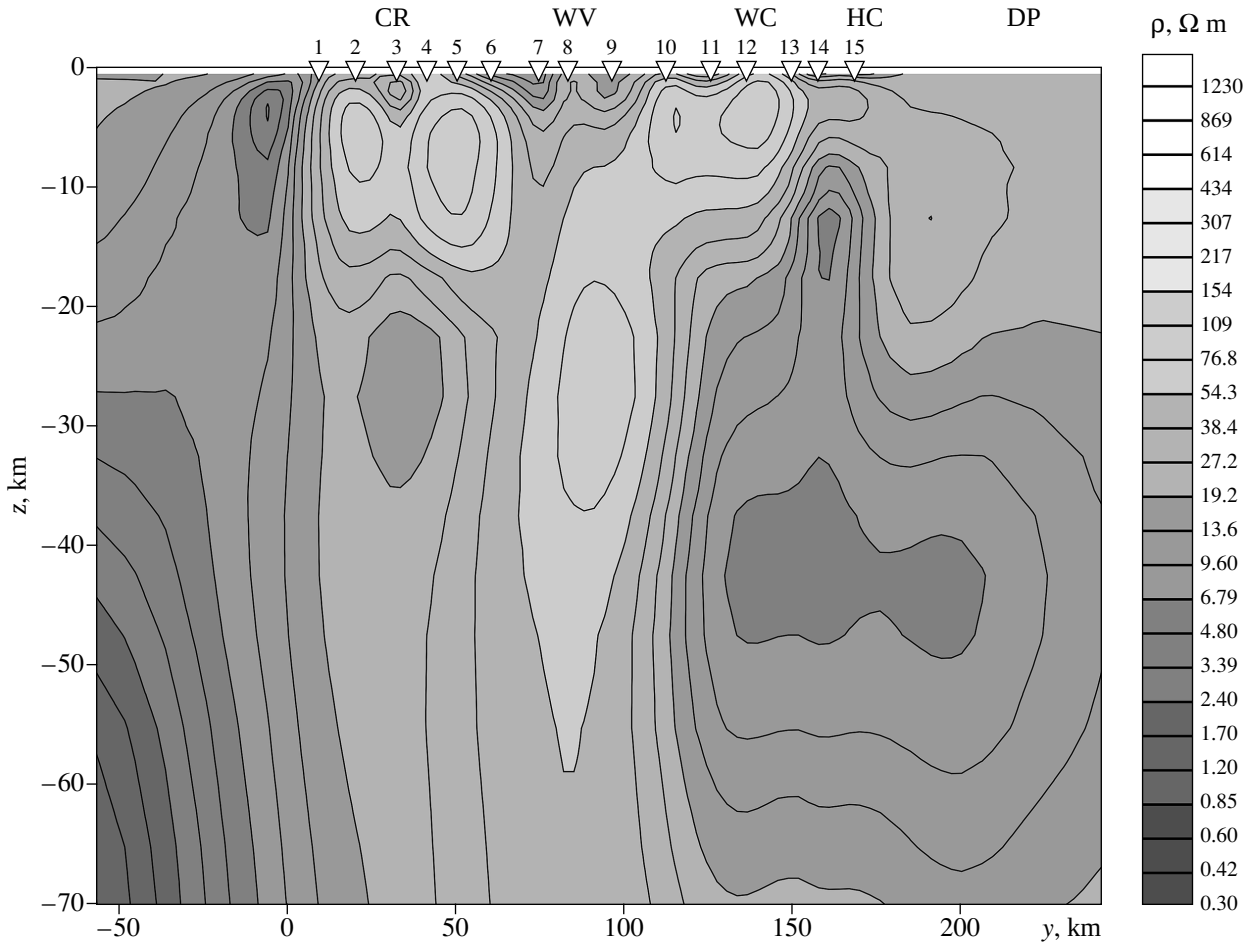

Fig. 18. The 2-D inversion of $\mathrm{Re}\,W_{zy}$, $\mathrm{Im}\,W_{zy}$, and $\varphi^{\parallel}$ performed with the use of the smoothing REBOCC program: CR, Coast Range; WV, Willamette Valley; WC, Western Cascades; HC, High Cascades; DP, Deschutes Plateau.

The EMSLAB-I model is open for criticism. A cold continental mantle contradicts current geodynamic ideas of the Cascadian subduction zone (compare the EMSLAB-I model with the predictive CASCADIA model shown in Fig. 16). Analysis of the EMSLAB-I model has shown that the TM-mode is weakly sensitive to variations in the electrical conductivity of the mantle and that the bimodal inversion alone, using both the TE and TM modes, can be effective in studying the asthenosphere [Berdichevsky *et al.*, 1992; Vanyan *et al.*, 2002].

Experiments on the bimodal interpretation of MTS and MVS data obtained in the Cascadian subduction zone resulted in the construction of the 2-D EMSLAB-II model (Fig. 17b). It was constructed with the use of the automatic inversion program INV2D-FG, optimizing resistivities on 20 blocks of a fixed geometry [Varentsov *et al.*, 1996]. An algorithm of parallel weighted inversion was applied to $\varphi^{\perp}$, $\mathrm{Re}\,W_{zy}$, and $\mathrm{Im}\,W_{zy}$ (maximum weight), $\varphi^{\parallel}$ and $\rho^{\perp}$ (normal weight), and $\rho^{\parallel}$ (minimum weight). The EMSLAB-II model has much in common with EMSLAB-I. Both have the same oceanic asthenosphere, subducting slab, and crustal conducting layer. However, the EMSLAB-II plate joins the crustal conductor, and a conducting asthenosphere is present in the EMSLAB-II continental mantle. Thus, the geoelectric data have revealed partial melting in the continental mantle. The main drawback of the EMSLAB-II model is its sketchiness due to the limited possibilities of the INV2D-FG program.

Presently, the INV2D-FG program has given way to more efficient software tools designed for the automatic 2-D inversion of MVS and MTS data. These are the smoothing program REBOCC [Siripunvaraporn and Egbert, 2000] and the programs IGF-MT2D [Nowozynski and Pushkarev, 2001] and II2DC [Varentsov, 2002]. These programs enable the optimization of models containing 512 and more blocks of a fixed geometry and provide new possibilities for interpreting the EMSLAB experimental data [Vanyan *et al.*, 2002].

Three-dimensional model estimates obtained for the Pacific coast of North America and analysis of experimental field characteristics, induction arrows, and polar diagrams show that the regional structure along the Lin-

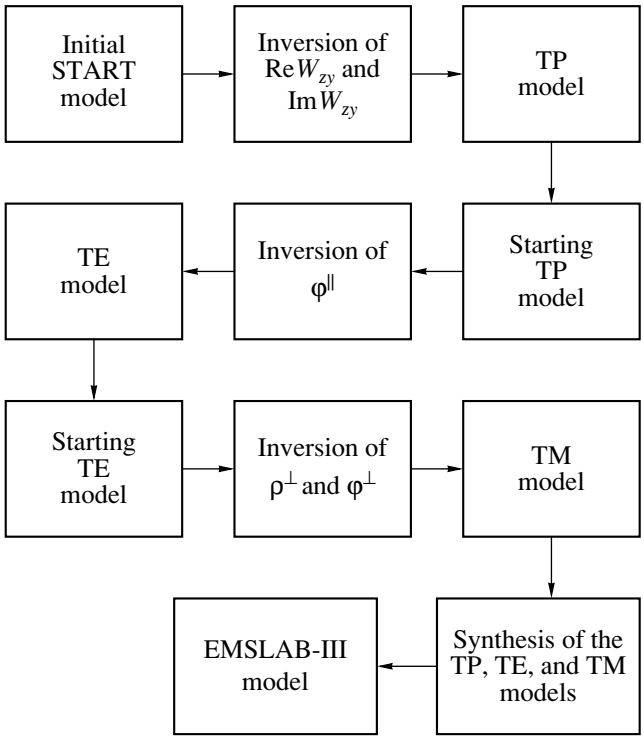

Fig. 19. Algorithm of interpretation of EMSLAB experimental data in the class of block models.

coln line is favorable for the 2-D interpretation of MVD and MTS data.

The interpretation consisted of three stages.

At the first stage, the 1-D inversion of short-period magnetotelluric (MT) curves (T = 0.01–100 s) was performed and an approximate geoelectric section of the continental volcanic-sedimentary cover was constructed to a depth of 3.5 km. This section agrees with the near-surface portion of the EMSLAB-I model [Wannamaker *et al.*, 1989b].

At the second stage, the REBOCC program was applied in experiments with 2-D smoothed inversion. With the complicated conditions of the Cascadian subduction zone, the parallel inversion of the TE- and TM-modes yielded whimsical alternation of low- and high-resistivity spots with a poor minimization of the misfit. It is difficult to recognize real structures of the subduction zone in these spots. The most interesting result was obtained from the partial inversion of $\mathrm{Re}\,W_{zy}$, $\mathrm{Im}\,W_{zy}$, and $\varphi^{\parallel}$ (Fig. 18). The western and eastern conducting zones identified here are separated by a T-shaped region of higher resistivity that can be associated with the subducting slab. An oceanic asthenosphere whose top can be fixed at a depth of about 30 km is recognizable in the western conducting zone. The eastern conducting zone coincides with the crust-mantle zone of wet melting in the predictive CASCADIA model shown in Fig. 16. It is noteworthy that the upper boundary of the eastern conductor closely resembles the topography of the crustal conducting zone in the EMSLAB-I and EMSLAB-II models shown in Fig. 17.

At the third, final stage, the method of partial inversions was applied and a new 2-D geoelectric model of the Cascadian subduction zone was constructed [Vanyan *et al.*, 2002]; this model was called EMSLAB-III. It was constructed with the use of the II2DC program [Varentsov, 2002], minimizing the model misfit in the class of media with a fixed geometry of blocks. The algorithm of interpretation consisting of partial inversions is illustrated in Fig. 19. The interpretation was conducted in the regime of testing hypotheses. We consider three hypotheses on the structure of the Cascadian subduction zone: (1) CASCADIA predictive model, (2) EMSLAB-I model, and (3) EMSLAB-II model.

The interpretation model is shown in Fig. 20a. The ocean floor topography and thicknesses of the seafloor, accretionary prism, and shelf sediments were specified from bathymetric and sedimentary thickness maps [Connard *et al.*, 1984a, 1984b]. The resistivities of the water, sediments, and oceanic crust were set at 0.3, 2, and 10 000 Ω m, respectively. The depth to the oceanic mantle and its resistivities were taken in accordance with the CASCADIA, EMSLAB-I, and EMSLAB-II models. The slab surface was constructed from seismic [Trehu *et al.*, 1994] and seismic tomography [Weaver and Michaelson, 1985; Rasmussen and Humphries, 1988] data. The structure of the volcanic-sedimentary cover was determined from the results of a 1-D inversion of short-period MT curves. The crust and mantle of

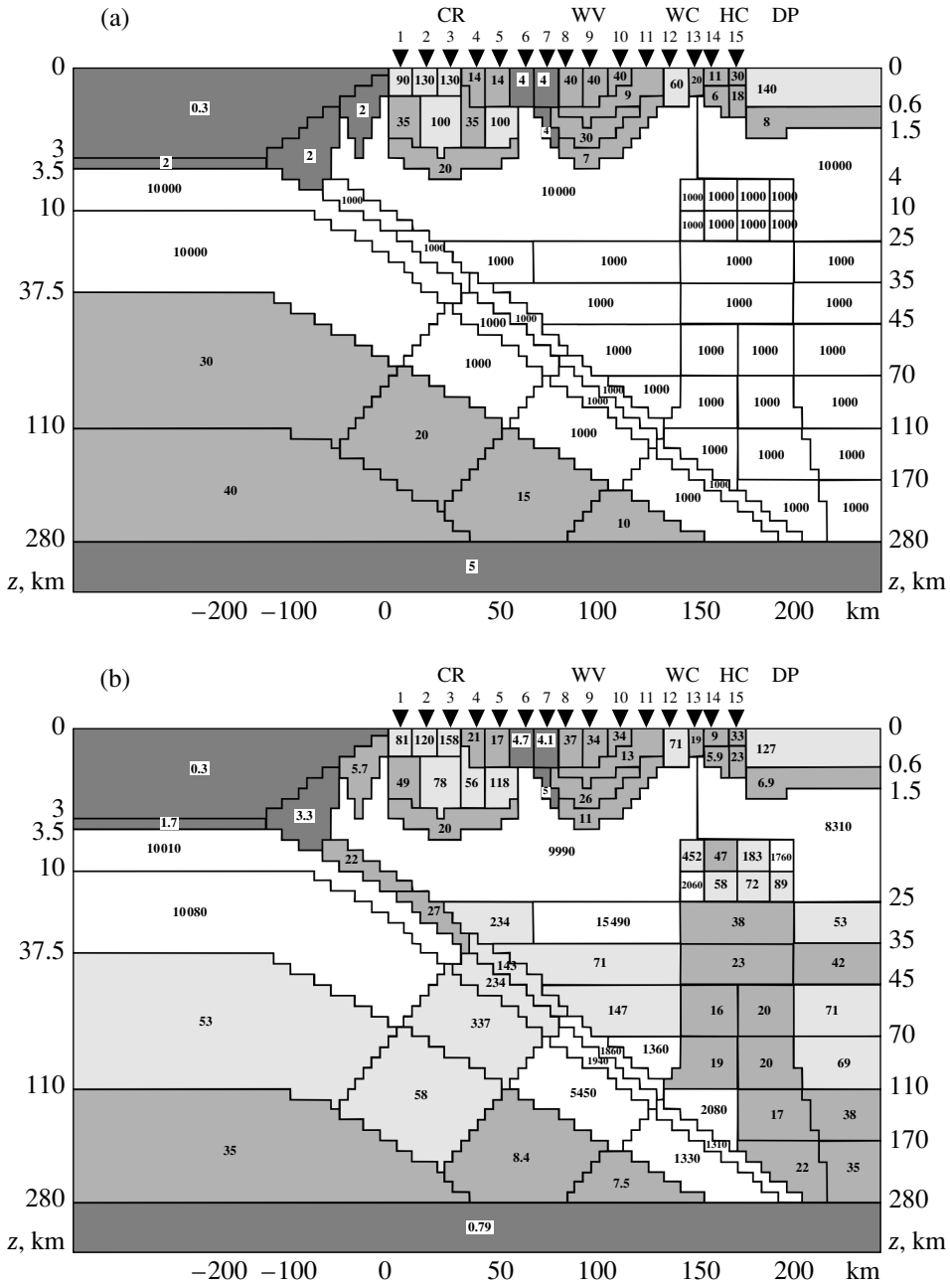

Fig. 20. Models obtained by partial inversions of the EMSLAB experimental data (resistivity values in units of Ω m are shown within blocks): (a) interpretation model (resistivity values of the initial START model are shown); (b) TP-2 model (inversion of $\mathrm{Re}\,W_{zy}$ and $\mathrm{Im}\,W_{zy}$); (c) TE model (inversion of $\varphi^{\parallel}$); (d) TM model (inversion of $\rho^{\perp}$ and $\varphi^{\perp}$). CR, Coast Range; WV, Willamette Valley; WC, Western Cascades; HC, High Cascades; DP, Deschutes Plateau.

the continent were divided into homogeneous blocks. The division density and block geometry were chosen with regard for the configuration of the eastern conducting zone, delineated with the help of the REBOCC program, and admitted a free choice of crust and mantle structures within the framework of the three hypotheses considered. A hypothesis best fitting the observed data is chosen automatically in the process of optimization of resistivities and minimization of misfits. The crust and mantle of the continent have a resistivity of 1000 Ω m in the starting START model constructed on the basis of the interpretation model. Below, we consider the successive partial inversions.

Inversion of $\mathrm{Re}\,W_{zy}$ and $\mathrm{Im}\,W_{zy}$. The START model was taken as the starting one. The TP model resulting from the inversion is shown in Fig. 20b. The tipper misfit (the rms deviation of model tippers from observed values) in this model is 5–10 times smaller than the tipper amplitude (the difference between the maximum and minimum tipper values), which is evidence of good

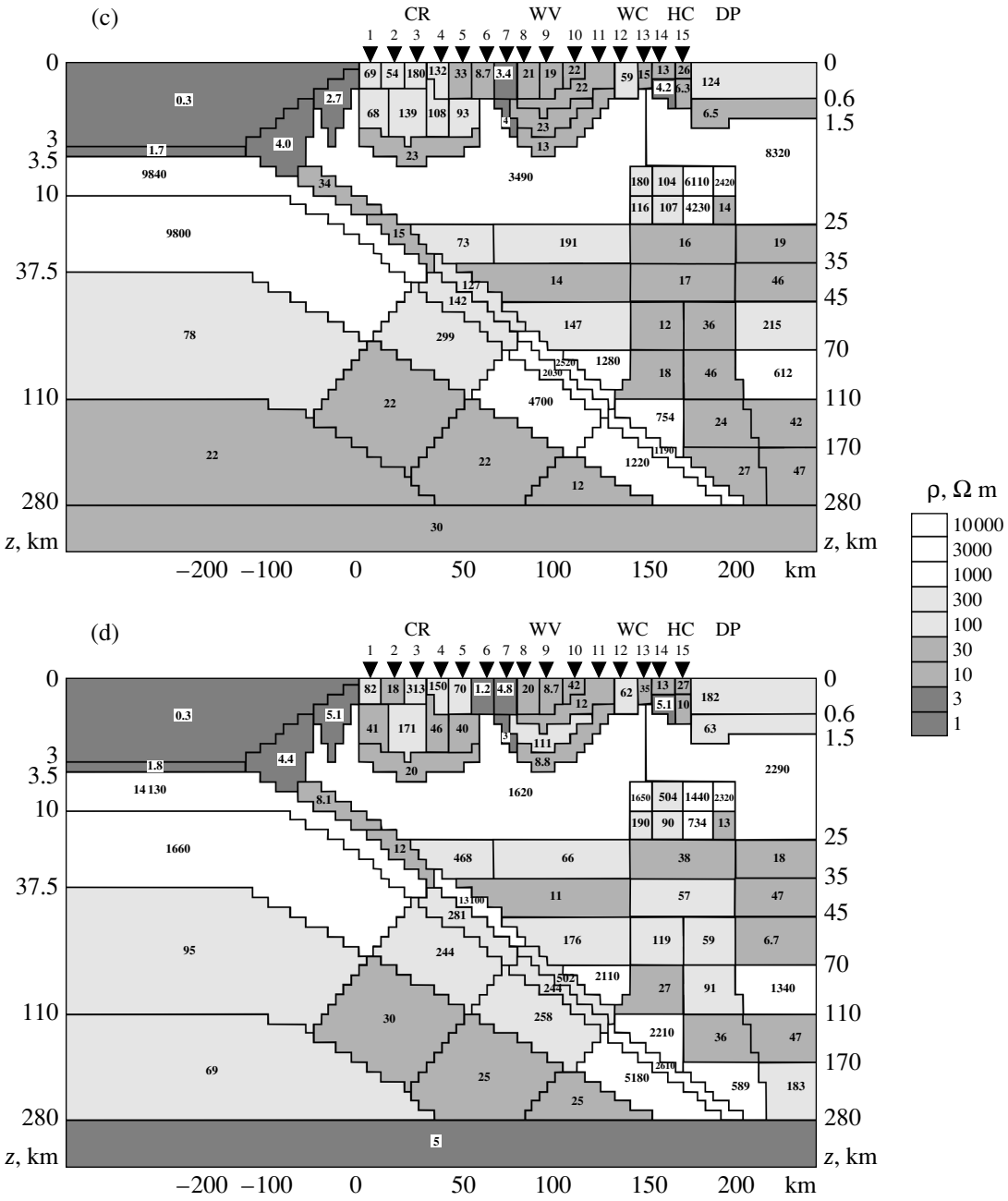

Fig. 20. (Contd.)

agreement of the model with observations. A remarkable feature of the TP model is the conducting continental asthenosphere and the vertical low-resistivity zone that branches from the asthenosphere and crosses the continental crust in the High Cascade region. This feature distinguishes the TP model from EMSLAB-I and EMSLAB-II and makes it similar to the predictive CASCADIA model; in the High Cascades, the latter delineates a vertical high-temperature zone of wet and dry melting that is evidently characterized by low resistivities.

Inversion of $\varphi^{\parallel}$. At this stage, we checked the tipper inversion results. To avoid difficulties related to near-surface distortions of the curves $\rho^{\parallel}$, we restricted ourselves to the inversion of the curves $\varphi^{\parallel}$, which satisfy the dispersion relations. The TP model, obtained from the tipper inversion, was used as a starting model. The inversion of longitudinal phases yielded the TE model, shown in Fig. 20c. The phase misfit (the rms deviation of model phases from observed values) in this model is 5–10 times smaller than the phase amplitude (the difference between the maximum and minimum phase values), indicating good agreement of the model with observations. As distinct from the TP model, the TE continental crust includes a better delineated conducting

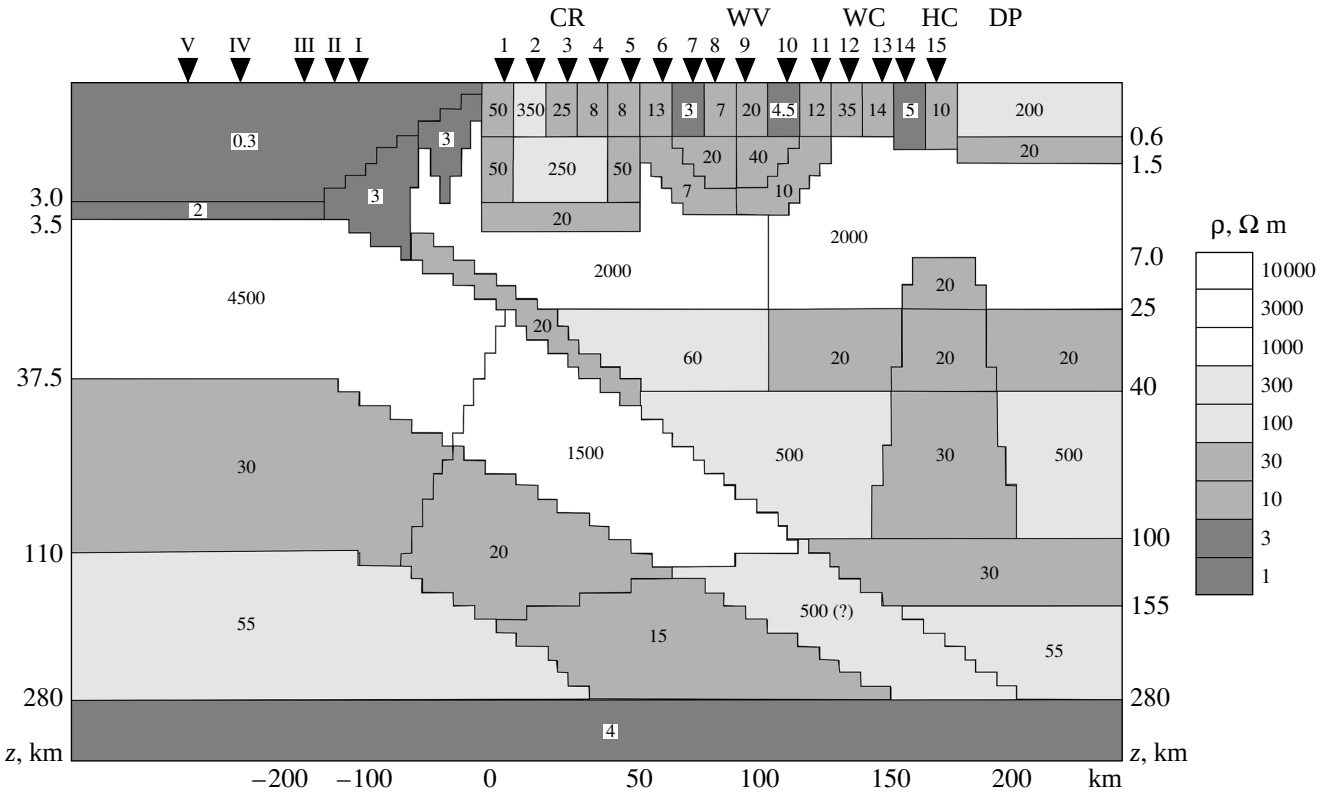

Fig. 21. Final EMSLAB-III model (resistivity values in units of Ω m are shown within blocks): I–V, soundings on the ocean floor; 1–15, soundings on the continent. CR, Coast Range; WV, Willamette Valley; WC, Western Cascades; HC, High Cascades; DP, Deschutes Plateau.

layer (ρ = 14–46 Ω m) in a depth interval of 35–45 km, whereas the subvertical conducting zone (ρ = 12–46 Ω m) in a depth interval of 45–110 km, bounded by layers with resistivities of 147–1260 Ω m to the west and 215–612 Ω m to the east, is localized with a higher contrast. One may state that the TE model is an updated TP model.

Inversion of $\rho^{\perp}$ and $\varphi^{\perp}$. At this stage, we inverted the TM-mode, which is less sensitive to conducting zones in the crust and mantle but is more effective in resolving the structure of the junction zone between the slab and crustal conducting layer and provides more reliable estimates of the resistivity in the upper consolidated crust. In inverting the TM-mode, the TE model, obtained from the inversion of phases $\varphi^{\parallel}$, was taken as a starting model. The inversion of transverse apparent resistivities and phases of the transverse impedance yielded the TM model shown in Fig. 20d. In this model, the misfits of transverse apparent resistivities at most points vary within 6–12%, and the phase misfits are 7–10 times smaller than the phase amplitude (the difference between the maximum and minimum phase values). The TM model inherits the main features of the starting TE model (albeit with some deviations). The following implications of the TM model are noteworthy. First, no well-conducting junction is present between the conducting slab and the crustal conducting layer. Second, the upper consolidated crust of the continent has a resistivity of about 2000 Ω m, indicating that it is fractured.

Note that the TM-mode inversion is essentially dependent on the choice of the starting model. If the START model is taken as the initial one, the TM-mode inversion yields a model in which the continental asthenosphere is absent. This is evidently due to the low sensitivity of the TM-mode to deep conducting structures. In this case, active is the same mechanism that gave rise to the model EMSLAB-I, devoid of the continental asthenosphere, in [Wannamaker *et al.*, 1989b].

Synthesis. At this stage, we analyzed the TP, TE, and TM models and constructed the general EMSLAB-III model, smoothing insignificant details and enlarging blocks on the basis of information characterizing the effect of individual blocks on the MVS and MTS characteristics. All changes were made in an interactive regime, with the calculation of local misfits and with the correction of boundaries and resistivities. The resulting general model shown in Fig. 21 provides a coherent geoelectric image of the subduction zone. The extent of its agreement with observed data is seen from Fig. 22, where the model curves $\rho^{\perp}$, $\rho^{\parallel}$, $\varphi^{\perp}$, $\varphi^{\parallel}$, $\mathrm{Re}\, W_{zy}$,

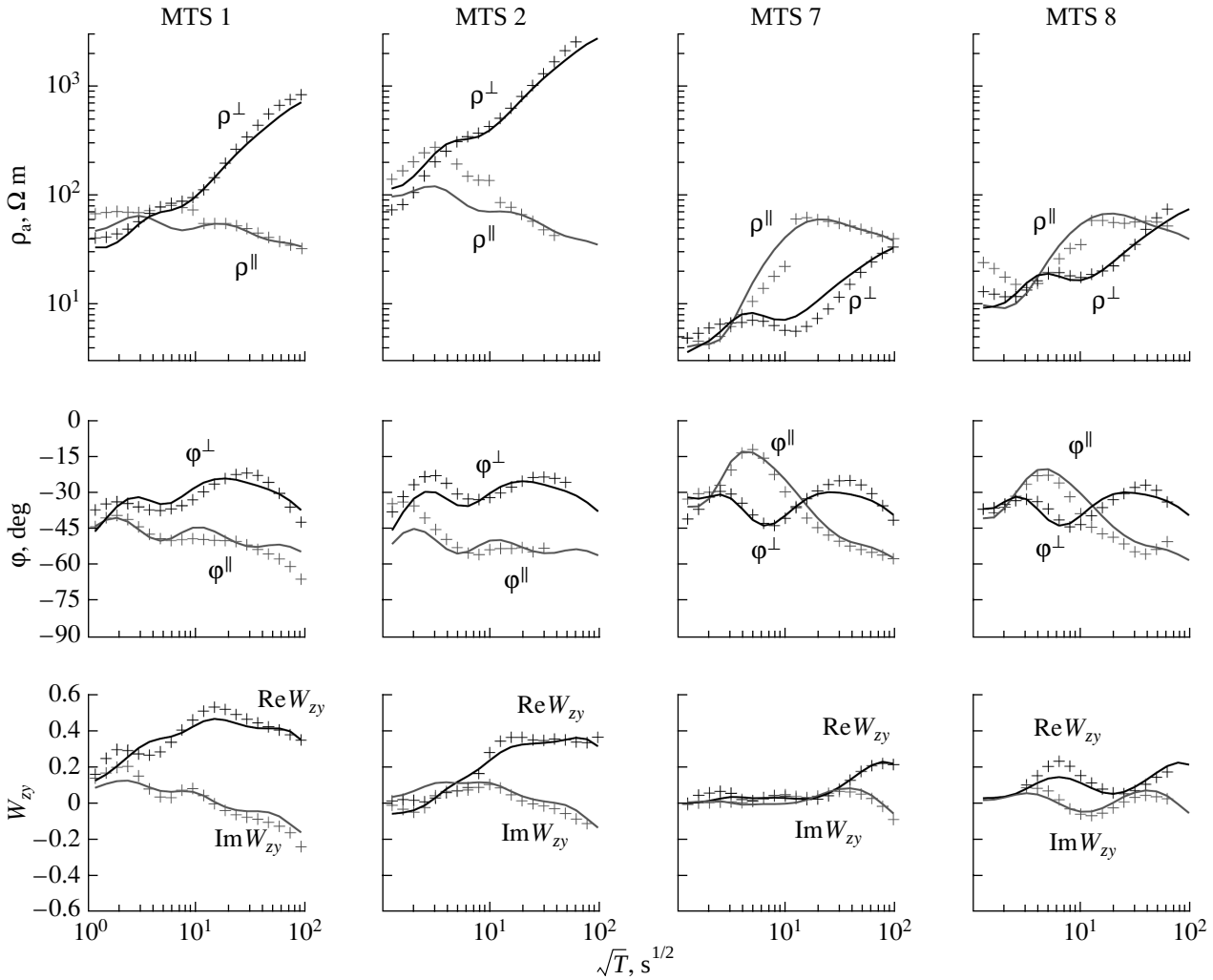

Fig. 22. Comparison of the observed MTS and MVS curves with the curves calculated from the EMSLAB-III model: (*1*) observations; (*2*) EMSLAB-III model.

and $\mathrm{Im}\,W_{zy}$ are compared with the observed curves (the static distortion in the observed curves $\rho^\parallel$ was removed by a vertical shift of their low-frequency branches). The model curves agree well with the observed curves at the majority of points.

In its oceanic part, the EMSLAB-III model is close to EMSLAB-I and EMSLAB-II and exhibits a thick oceanic asthenosphere in a depth interval of 37.5–110 km. The structure of the continental part of EMSLAB-III is distinguished by the following significant elements:

a crustal conducting layer (ρ = 20 Ω m, a depth interval of 25–40 km) and a conducting asthenosphere (30 Ω m, 100–155 km) are distinctly resolved;

the crustal and asthenospheric conductors are connected by a columnlike conducting body (20–30 Ω m) crossing the lithosphere and reaching depths of about 7 km in the volcanic zone of the High Cascades;

the subducting slab, in a depth interval of 4–40 km contains a thin inclined conductor (20 Ω m) separated from the crustal conducting layer by a higher-resistivity zone (60 Ω m); apparently, the crustal conducting layer is unrelated to slab fluids and has a deep origin.

The reliability of these elements is supported by the fact that the elimination of any of them noticeably increases the model misfits.

These features of the continental section make the EMSLAB-III and predictive CASCADIA models similar. The fluid regime of the subduction zone is clearly observable here. The subducting slab entraps fluid-saturated low-resistivity rocks of the ocean floor. As the slab moves down, the released free water migrates through the shear zone (the contact zone between the subducting oceanic and stable continental plates). The dehydration (the release of bound water) developing in the slab at depths of 30–40 km supplies fluids to the mantle and causes the wet melting of asthenospheric material. The low-resistivity melts move upward

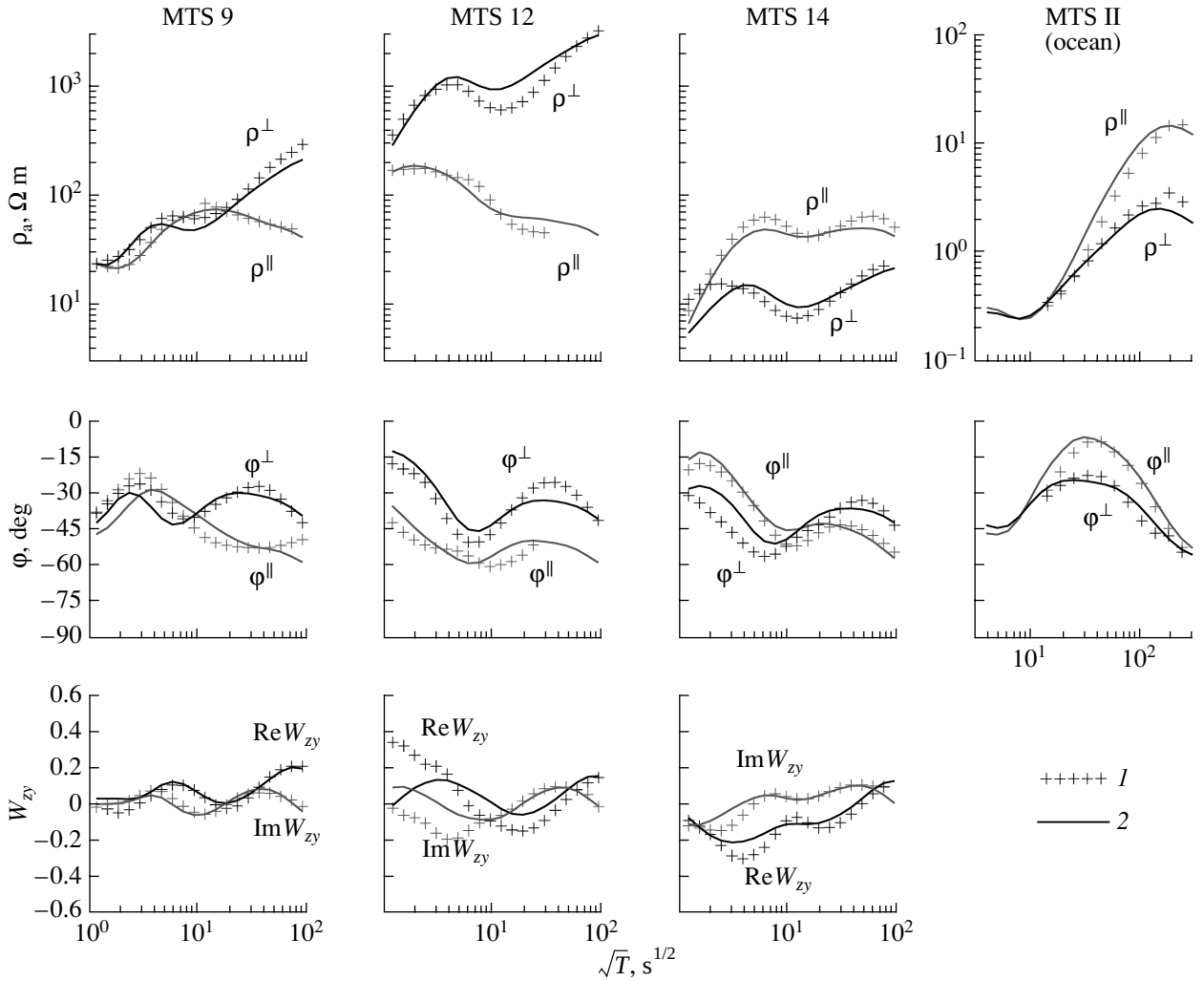

Fig. 22. (Contd.)

through the lithosphere and form a volcanic arc. The heating of the lithosphere activates dehydration in the lower crust, producing the crustal conducting layer.

All this confirms the validity of the predictions underlying the CASCADIA model.

CONCLUSION

Theoretical and experimental results indicate that the MVS method can play a significant role in the development of geoelectric studies. Its main advantage consists in the fact that the magnetic field distortions caused by near-surface inhomogeneities attenuate with decreasing frequency and do not spoil the information on structures of the crust and upper mantle. This makes the results of electromagnetic studies more reliable and better constrained. The development of the MVS method should be regarded as a promising problem of modern geophysics.

Presently, we are at the very beginning of this research, and many questions remain unanswered. What is the best way to organize qualitative analysis of MVS data that accounts most adequately for horizontal and vertical variations in the electrical conductivity? What is the resolution of tippers with respect to these variations? How rapidly do the magnetovariational near-surface effects attenuate at low frequencies? What is the sensitivity of tippers to deep structures in the crust and mantle? Which geoelectric conditions are favorable for the application of the MVS method? What are the conditions at which tippers admit a 2-D approximation of 3-D structures? Such is the list of problems, far from being complete, whose solution is crucial for the progress of MVS.

Answers to many questions can be obtained with the further accumulation of experience in studies in various geological provinces. Here, we should emphasize that a necessary condition for the MVS application is the

presence of conducting inhomogeneities that play the role of deep local sources of electromagnetic field.

The main goal of this paper was to attract the attention of geophysicists to the potentialities of the MVS method and to problems whose solution is indispensable to the practical realization of these potentialities.

ACKNOWLEDGMENTS

We are grateful to P. Weidelt and U. Schmucker for discussions stimulating this work. This work was supported by the Russian Foundation for Basic Research, project nos. 02-05-64079 and 03-05-64167.

REFERENCES

Bahr, K., Interpretation of Magnetotelluric Impedance Tensor: Regional Induction and Local Telluric Distortion, *J. Geophys.*, 1988, vol. 62, pp 119–127.

Berdichevsky, M.N. and Zhdanov, M.S., *Advanced Theory of Deep Geomagnetic Sounding*, Amsterdam: Elsevier, 1984.

Berdichevsky, M.N. and Dmitriev, V.I., *Magnitotelluricheskoe zondirovanie gorizontal'no-odnorodnykh sred* (Magnetotelluric Sounding of Horizontally Homogeneous Media), Moscow: Nedra, 1991.

Berdichevsky, M.N., Koldaev, D.S., and Yakovlev, A.G., Magnetotelluric Sounding on an Ocean Coast, *Fiz. Zemli*, 1992, no. 6, pp. 87–96.

Berdichevsky, M.N., Dmitriev, V.I., and Pozdnjakova, E.E., On Two-Dimensional Interpretation of Magnetotelluric Soundings, *Geophys. J. Int.*, 1998, vol. 133, pp. 585–606.

Berdichevsky, M.N., Vanyan, L.L., and Koshurnikov, A.V., Magnetotelluric Sounding in the Baikal Rift Zone, *Izvestiya, Phys. Solid Earth*, 1999, vol. 35, pp. 793–814.

Berdichevsky, M.N. and Dmitriev, V.I., *Magnetotellurics in the Context of the Theory of Ill-Posed Problems*, Tulsa: SEG, 2002.

Bur'yanov, V.B., Gordienko, V.V., Kulik, S.N., and Logvinov, I.M., *Kompleksnoe geofizicheskoe izuchenie tektonosfery kontinentov* (Multidisciplinary Geophysical Study of the Continental Tectonosphere), Kiev: Naukova Dumka, 1983.

Caldwell, T.G., Bibby, H.M., and Brown, C., The Magnetotelluric Phase Tensor—A Method of Distortion Analysis for 3D Regional Conductivity Structures, *Abstracts of 16th Workshop on EM Induction in the Earth*, Santa Fe, EM12-4.

Connard, G., Couch, R., Keeling, K., *et al.*, Abyssal Plain and Continental Net-Objective Sedimentary Thickness, *Western North American Continental Margin and Adjacent Ocean Floor off Oregon and Washington. Atlas 1 Ocean Margin Drilling Program*, L.D. Kulm *et al.*, Eds., Regional Atlas Series: Marine Science International, Sheet 7, 1984a.

Connard, G., Couch, R., Pitts, G.S., and Troseth, S., Bathymetry and Topography, *Western North American Continental Margin and Adjacent Ocean Floor off Oregon and Washington. Atlas 1 Ocean Margin Drilling Program*, L.D. Kulm *et al.*, Eds., Regional Atlas Series: Marine Science International. Sheet 1, 1984b.

Dmitriev, V.I., *Elektromagnitnye polya v neodnorodnykh sredakh* (Electromagnetic Fields in Inhomogeneous Media), Moscow: MGU, 1969.

Dmitriev, V.I., Inverse Problems in Electrodynamical Prospecting, *Ill-Posed Problems in the Natural Sciences*, Moscow: Mir Publishers, 1987, pp. 77–101.

Dmitriev, V.I. and Mershchikova, N.A., Synthesis of the Magnetotelluric Field, *Fiz. Zemli*, 2002, no. 11, pp. 69–75.

Groom, R.W. and Bailey, R.C., Decomposition of Magnetotelluric Impedance Tensor in the Presence of Local Three-Dimensional Galvanic Distortion, *J. Geophys. Res.*, 1989, vol. 94, no. B2, pp. 1913–1925.

Gusarov, A.L., On the Uniqueness of the Magnetotelluric Data Inversion in a Two-Dimensional Medium, *Matematicheskie modeli v geofizike* (Mathematical Models in Geophysics), Moscow: MGU, 1981, pp. 31–61.

Jones, A.G., Static Shift of Magnetotelluric Data and Its Removal in a Sedimentary Basin Environment, *Geophysics*, 1988, vol. 53, no. 7, pp. 967–978.

Nowozynski, K. and Pushkarev, P.Yu., The Efficiency Analysis of Programs for Two-Dimensional Inversion of Magnetotelluric Data, *Izvestiya, Physics of the Solid Earth*, 2001, vol. 37, pp. 503–516.

Osipova, I.L., Berdichevsky, M.N., Vanyan, L.L., and Borisova, V.P., Geoelectric Models of North America, *Geomagn. Issled.*, 1982, no. 29, pp. 117–130.

Pous, J., Queralt, P., and Marcuello, A., Magnetotelluric Signature of the Western Cantabrian Mountains, *Geophys. Res. Lett.*, 2001, vol. 28, no. 9, pp. 1795–1798.

Rasmussen, J. and Humphries, G., Tomographic Image of the Juan de Fuca Plate beneath Washington and Western Oregon Using Teleseismic *P*-Wave Travel Times, *Geophys. Res. Lett.*, 1988, no. 15, pp. 1417–1420.

Roecker, S.W., Sabitova, T.M., Vinnik, L.P., *et al.*, Three-Dimensional Elastic Wave Velocity Structure of Western and Central Tien Shan, *J. Geophys. Res.*, 1993, vol. 98, no. B9, pp. 15 579–15 795.

Rokityansky, I.I., *Geoelectromagnetic Investigations of the Earth's Crust and Mantle*, Berlin: Springer, 1982.

Romanyuk, T.V., Mooney, W.D., and Blakely, R.J., A Tectonic–Geophysical Model of the Cascadian Subduction Zone in North America, *Geotektonika*, 2001, no. 3, pp. 88–110.

Siripunvaraporn, W. and Egbert, G., An Efficient Data Subspace Inversion Method for 2-D Magnetotelluric Data, *Geophysics*, 2000, vol. 65, pp. 791–803.

Trapeznikov, Yu.A., Andreeva, E.V., Batalev, V.Yu., *et al.*, Magnetotelluric Sounding in the Kyrgyz Tien Shan, *Fiz. Zemli*, 1997, no. 1, pp. 3–20.

Trehu, A.M., Asudeh, I., Brocher, T.M., *et al.*, Crustal Architecture of the Cascadia Forearc, *Science*, 1994, vol. 265, pp. 237–243.

Vanyan, L.L., *Osnovy elektromagnitnykh zondirovanii* (Fundamentals of Electromagnetic Sounding), Moscow: Nedra, 1965.

Vanyan, L.L., Varentsov, I.M., Golubev, N.G., and Sokolova, E.Yu., Construction of Induction Magnetotelluric Curves from Profile Geomagnetic Data for the Study of Electrical Conductivity of the Continental Asthenosphere in the EMSLAB Experiment, *Fiz. Zemli*, 1997, no. 10, pp. 33–46.

Vanyan, L.L., Varentsov, I.M., Golubev, N.G., and Sokolova, E.Yu., Derivation of Simultaneous Geomagnetic Field Components from Tipper Arrays, *Izvestiya, Physics of the Solid Earth*, 1998, vol. 34, pp. 779–786.

Vanyan, L.L., Berdichevsky, M.N., Pushkarev, P.Yu., and Romanyuk, T.V., A Geoelectric Model of the Cascadia Subduction Zone, *Izvestiya, Physics of the Solid Earth*, 2002, vol. 38, pp. 816–845.

Varentsov, I.M., A General Approach to the Magnetotelluric Data Inversion in a Piecewise-Continuous Medium, *Izvestiya, Physics of the Solid Earth*, 2002, vol. 38, pp. 913–934.

Varentsov, I.M., Golubev, N.G., Gordienko, V.V., and Sokolova, E.Yu., Study of the Deep Geoelectric Structure along the Lincoln Line (EMSLAB Experiment), *Fiz. Zemli*, 1996, no. 4, pp. 124–144.

Vozoff, K., The Magnetotelluric Method, *Electromagnetic Methods in Applied Geophysics*, Tulsa: SEG, 1991, vol. 2, pp. 641–711.

Wannamaker, P.E., Stodt, J.A., and Rijo, L., A Stable Finite Element Solution for Two-Dimensional Magnetotelluric Modeling, *Geophys. J. R. Astron. Soc.*, 1987, vol. 88, pp. 277–296.

Wannamaker, P.E., Booker, J.R., Filloux, J.H., *et al.*, Magnetotelluric Observations across the Juan de Fuca Subduction System in the EMSLAB Project, *J. Geophys. Res.*, 1989a, vol. 94, no. B10, pp. 14 111–14 125.

Wannamaker, P.E., Booker, J.R., Jones, A.G., *et al.*, Resistivity Cross Section through the Juan de Fuca Subduction System and Its Tectonic Implications, *J. Geophys. Res.*, 1989b, vol. 94, no. B10, pp. 14 127–14 144.

Weaver, C.S. and Michaelson, C.A., Seismicity and Volcanism in the Pacific Northwest: Evidence for the Segmentation of the Juan de Fuca Plate, *Geophys. Res. Lett.*, 1985, vol. 12, pp. 215–218.

Zinger, B.Sh., Corrections for Distortions of Magnetotelluric Fields: Limits of Validity and Static Approach, *Surv. Geophys.*, 1992, vol. 57, pp. 603–622.